




# The Effect of Weak Resistivity and Weak Thermal Diffusion on Short-wavelength Magnetic Buoyancy Instability

Marek J. Gradzki  and Krzysztof A. Mizerski 

Department of Magnetism, Institute of Geophysics, Polish Academy of Sciences, ul. Księcia Janusza 64, 01–452 Warsaw, Poland  
[mgradzki@igf.edu.pl](mailto:mgradzki@igf.edu.pl), [kamiz@igf.edu.pl](mailto:kamiz@igf.edu.pl)

Received 2017 October 23; revised 2017 December 20; accepted 2017 December 20; published 2018 March 2

## Abstract

Magnetic buoyancy instability in weakly resistive and thermally conductive plasma is an important mechanism of magnetic field expulsion in astrophysical systems. It is often invoked, e.g., in the context of the solar interior. Here, we revisit a problem introduced by Gilman: the short-wavelength linear stability of a plane layer of compressible isothermal and weakly diffusive fluid permeated by a horizontal magnetic field of strength decreasing with height. In this physical setting, we investigate the effect of weak resistivity and weak thermal conductivity on the short-wavelength perturbations, localized in the vertical direction, and show that the presence of diffusion allows to establish the wavelength of the most unstable mode, undetermined in an ideal fluid. When diffusive effects are neglected, the perturbations are amplified at a rate that monotonically increases as the wavelength tends to zero. We demonstrate that, when the resistivity and thermal conduction are introduced, the wavelength of the most unstable perturbation is established and its scaling law with the diffusion parameters depends on gradients of the mean magnetic field, temperature, and density. Three main dynamical regimes are identified, with the wavelength of the most unstable mode scaling as either  $\lambda/d \sim \mathcal{U}_\kappa^{3/5}$  or  $\lambda/d \sim \mathcal{U}_\kappa^{3/4}$  or  $\lambda/d \sim \mathcal{U}_\kappa^{1/3}$ , where  $d$  is the layer thickness and  $\mathcal{U}_\kappa$  is the ratio of the characteristic thermal diffusion velocity scale to the free-fall velocity. Our analytic results are backed up by a series of numerical solutions. The two-dimensional interchange modes are shown to dominate over three-dimensional ones when the magnetic field and/or temperature gradients are strong enough.

*Key words:* instabilities – magnetic fields – magnetohydrodynamics (MHD) – sunspots

## 1. Introduction

The instability triggered by magnetic flux tubes that locally decrease the gas density, thus creating buoyancy, has been known since Parker (1955) and Newcomb (1961). The requirement for this type of instability to develop in compressible plasma is the stratification of horizontal magnetic fields. Since their discovery, the magnetic buoyancy instabilities have been invoked numerous times in astrophysics in the context of stars, accretion disks, and interstellar medium (cf. Parker 1979 and Choudhuri 1998). In particular, according to, e.g., Hughes (2007), They seem to be a promising candidate for the mechanism of break-up and escape of a predominantly toroidal magnetic field from the solar tachocline, which is then dragged by the flow in the convection zone toward the Sun’s surface, where it appears as active regions. Motivated by magnetic field dynamics in the tachocline, we return to the pioneering work of Gilman (1970), who studied the magnetic buoyancy instability in the solar context, while neglecting all diffusive processes, i.e., viscosity, the fluid’s resistivity and thermal conduction, which are indeed very weak in the Sun’s interior. He showed that the most rapidly growing perturbations are short-wavelength in the horizontal direction, perpendicular to the imposed, stratified horizontal magnetic field, which was later confirmed by Acheson (1979). That work was recently followed by Mizerski et al. (2013), who studied the same idealized model of Gilman (1970) with the use of the Rayleigh–Schrödinger asymptotic approach in the limit of short perturbational wavelengths. They found the growth rate and structure of the most unstable mode—however, they were unable to determine the finite magnitude of its wavelength,

because the most unstable mode turns out to be the one with infinite wavenumber in the absence of dissipation.

The magnetic buoyancy was studied in a broader context by Cattaneo et al. (1990) and Hughes (1992), who described its possible role in the formation of sunspots and in the solar dynamo cycle. On the other hand, the effect of magnetic buoyancy in magnetoconvection was studied by Hughes & Proctor (1988), while the influence of shear was examined by Tobias & Hughes (2004) and more recently by Bowker et al. (2014). The joint effect of rotation and magnetic buoyancy was investigated by Hughes (1985), while the possible large-scale dynamo action triggered by the magnetic buoyancy instability was studied by Davies & Hughes (2011), who calculated the mean electromotive force induced by the instability.

A number of interesting results from numerical simulations have also been reported. Cattaneo & Hughes (1988) studied the nonlinear break-up of a magnetic layer, particularly in the context of the instability of interchange modes. In a somewhat wider context, the nonlinear evolution of the magnetic buoyancy instability was investigated by Kersal et al. (2007). Berkoff et al. (2010) compared the anelastic approximation with the fully compressible equations for linear magnetoconvection and flow driven by the magnetic buoyancy effect.

Magnetic buoyancy instability was also considered in the context of the Terrestrial magnetic field by Acheson (1980, 1983) and Friedlander (1987). It was shown to influence the propagation of magneto-gravitational waves by changing their Brunt–Väisälä frequency and destabilizing them, thus influencing the oscillations of the geomagnetic field.

The aim of this paper is to explain how the wavelength of the fastest-growing perturbation is established by the presence of magnetic and thermal diffusivity (which seem to be most

important in the astrophysical context); in other words, at which wavenumber magnitude the diffusive decay starts to dominate and the growth rate starts to decrease with decreasing wavelength. We follow the approach of Mizerski et al. (2013) and apply the same asymptotic techniques. Several different regimes are identified, which leads to quite diverse results. In order to clearly classify all the possible regimes and minimize the complexity of the cumbersome analytic calculations, we consider only the most unstable modes; strongly oscillatory solutions identified in Mizerski et al. (2013), which are never the fastest-growing modes, are not presented. Moreover, for the sake of clarity, we also consider only the so-called “body modes,” i.e., the most unstable perturbations that develop in the interior of the domain, as opposed to the “wall modes,” which can develop near the boundaries under certain circumstances. We also take advantage of the results of Mizerski et al. (2013), who clearly showed how to approach the “wall modes” (the approach being nearly the same as for “body modes”), and thus our results can be easily generalized to the case wherein the most unstable modes develop in the vicinity of boundaries. Moreover, the oscillatory modes can also be found via the WKB technique, in the same fashion as in Mizerski et al. (2013), who have also performed numerical simulations of evolution of the non-dissipative system from some initial state, localized far from the growth rate maximum. They showed that the boundary layer (BL)-type mode localized near the growth rate maximum eventually dominates all others; however, it must be said that, in the nonlinear regime, all the modes from the spectrum would necessarily interact. Due to the local nature of the instability it is possible, that an initial perturbation localized far from the growth rate maximum could grow to a magnitude large enough to put the system in a nonlinear regime, even before the most unstable mode could take over. Nevertheless, due to the possibility for simple generalization of the results obtained here to other types of modes (for which the detailed analysis can be found in Mizerski et al. (2013) and easily repeated), for the sake of clarity, we concentrate here on only the most unstable modes. In many applications, however, it is in fact the most unstable mode that is most relevant, because it is likely to dominate the dynamics.

Let us also mention that, from an astrophysical point of view, we are considering a very simplified setting because the influence of shear, which is vital in the context of the tachocline (cf. Hughes 2007), is neglected here. Moreover, the effect of the baroclinic instabilities, emphasized by Gilman (1967a, 1967b, 1967c, 1967d, 2014, 2015, 2017) is also not included. However, this paper presents a clear study of the complicated influence of weak resistivity and weak thermal conduction on the magnetic buoyancy instability, so for the sake of clarity, it is crucial to isolate this effect from other complex aspects of the true dynamics (the results obtained here are reached in different regimes and scalings for the wavenumber of the most unstable mode with the diffusivities, and are clearly categorized). Nevertheless, because the magnetic buoyancy is strongly relevant to solar tachocline, we think it is worthwhile to comment on the parameter regime that pertains to the tachocline in this paper.

The paper is organized as follows. The governing equations describing the magnetic buoyancy instability of a layer of gas with a vertically stratified horizontal magnetic field are provided in Section 2. For simplicity, we first restrict our attention to two-dimensional (interchange) perturbations, for

which the magnetic field remains unidirectional. In Section 3, we analyze the effect of electric resistivity alone, i.e., in an isothermal fluid (with infinitely fast thermal relaxation), within the asymptotic limit of small ratio of the free-fall timescale to the resistive one. In Section 4, a similar asymptotic analysis is carried out to study the joint effect of the resistivity and thermal diffusion, with the latter much greater than the former, as expected from estimates of physical parameter values at the bottom of the solar convection zone, provided by Gough (2007). Three distinct dynamical regimes are found and thoroughly described in a short summary at the end of that section. The joint influence of both diffusivities turns out to be crucial in some cases, as the sole effect of thermal diffusion is negligible for sufficiently weak mean temperature gradients. In Section 5, we present the numerical solutions of the linear stability equations and report a good agreement with the asymptotic results of previous sections. In Section 6, we show how the high-wavenumber analysis carries over to the case of fully three-dimensional perturbations, and a final recipe for determination of the most unstable mode in the analyzed system is provided in 6.3. Our concluding discussion is contained in Section 7.

## 2. Mathematical Formulation

We consider a plane layer of thickness  $d$ , filled with inviscid, compressible, and electrically and thermally conducting fluid, described by the perfect gas equation of state in the presence of an external, horizontal magnetic field. We assume that the boundaries are perfect electric conductors. The system of evolution equations for this physical setting, for the velocity  $\mathbf{u}$ , magnetic field  $\mathbf{B}$ , density  $\rho$ , pressure  $p$ , and temperature  $T$ , consists of the Navier–Stokes, magnetic induction, temperature, and continuity equations, supplied by the state equation of an ideal gas and Gauss’s law for magnetism. These are expressed in the following nondimensional form:

$$\rho \frac{\partial}{\partial t} \mathbf{u} + \rho (\mathbf{u} \cdot \nabla) \mathbf{u} = -\mathcal{P} \nabla p + \Lambda (\nabla \times \mathbf{B}) \times \mathbf{B} - \rho \hat{\mathbf{e}}_z, \quad (1a)$$

$$\frac{\partial}{\partial t} \mathbf{B} + (\mathbf{u} \cdot \nabla) \mathbf{B} = (\mathbf{B} \cdot \nabla) \mathbf{u} - \mathbf{B} (\nabla \cdot \mathbf{u}) + \mathcal{U}_\eta \nabla^2 \mathbf{B}, \quad (1b)$$

$$\begin{aligned} \rho \frac{\partial}{\partial t} T + \rho \mathbf{u} \cdot \nabla T &= \gamma \mathcal{U}_\kappa \nabla^2 T - \frac{\gamma - 1}{\alpha} (\nabla \cdot \mathbf{u}) p \\ &+ \frac{\gamma - 1}{\alpha} \mathcal{U}_\eta \frac{\Lambda}{\mathcal{P}} (\nabla \times \mathbf{B})^2, \end{aligned} \quad (1c)$$

$$\frac{\partial}{\partial t} \rho + \nabla \cdot (\rho \mathbf{u}) = 0, \quad (1d)$$

$$p = \alpha \rho T, \quad (1e)$$

$$\nabla \cdot \mathbf{B} = 0, \quad (1f)$$

where

$$\mathcal{P} = \frac{p_s}{\rho_s g d}, \quad \alpha = \frac{R \rho_s T_s}{p_s}, \quad \Lambda = \frac{B_s^2}{\mu_0 \rho_s g d} = \beta^{-1} \mathcal{P}, \quad (2a)$$

$$\mathcal{U}_\eta = \frac{\eta}{d \sqrt{g d}}, \quad \mathcal{U}_\kappa = \frac{\kappa}{d \sqrt{g d}}, \quad (2b)$$

and  $p_s, \rho_s, T_s, B_s$  are the scales of pressure, density, temperature, and the magnetic field, respectively. Plasma  $\beta$  is the ratio of the gas pressure to the magnetic pressure:  $\beta = \mu_0 p_s / B_s^2$ ,  $\mu_0$  is the

vacuum permeability, and  $\gamma = c_p/c_v$  the specific heats ratio. For the units of length, time, and velocity, we chose the layer thickness  $d$ , the free fall time  $\sqrt{d/g}$ , and the freefall velocity  $\sqrt{gd}$ , respectively. The acceleration of gravity  $g$ , magnetic diffusivity  $\eta$ , thermal conductivity  $k = \kappa c_p \rho_s$ , and specific heats  $c_p$  and  $c_v$  are assumed constant. Despite exclusion of shear, which is significant in the solar tachocline, we will make some references to the tachocline in the local context; i.e., we adopt a Cartesian coordinate system for our model, in which positive  $x$  points east,  $y$  points north, and  $z$  points radially (in the direction opposite to gravity).

As advertised in the introduction, in order to thoroughly study the effect of diffusion on the short-wavelength magnetic buoyancy instability, two separate cases will be considered: (i) isothermal with asymptotically small, dimensionless magnetic diffusivity  $\mathcal{U}_\eta$  (Section 3), and (ii) non-isothermal with both diffusivities, thermal  $\mathcal{U}_\kappa$ , and magnetic  $\mathcal{U}_\eta$  asymptotically small, and with an assumed scaling  $\mathcal{U}_\eta \sim \mathcal{U}_\kappa^{3/2}$  that pertains to the tachocline (Section 4).

We neglect here the effect of rotation, because the Sun is a slowly rotating star and the magnitude of the Coriolis term measured by the ratio of rotational speed to the freefall velocity is on the order  $10^{-4}$  (cf. physical parameter values for the tachocline provided by Gough 2007) within the framework of the adopted set of dimensional scales. Thus, we feel it is fully justified to neglect the Sun's rotation in the leading-order analysis, although its effect should be included in possible future studies concerning magnetic dynamo induced by magnetic buoyancy, as it might be important in the process of generation of a large-scale poloidal field.

### 3. Influence of Magnetic Diffusivity

Let us first treat the simplest case. Assume now that the system is a conducting fluid with magnetic diffusivity  $\mathcal{U}_\eta \ll 1$ . We assume further that the system is isothermal. Thus, we do not need the temperature Equation 1(c), and the parameter  $\alpha$  contains the constant temperature  $T$  of the system. Under these assumptions, we will now investigate the role of resistivity in the dynamics of magnetic buoyancy instability.

To determine the basic state from Equations 1(a)–(f), which will later be perturbed, we consider a layer of stationary fluid in equilibrium, in dimensionless region  $0 \leq z \leq 1$ , with a horizontal  $z$ - and time-dependent magnetic field,

$$\bar{\mathbf{B}}_t = \bar{B}_t(z, t) \hat{e}_x, \quad (3)$$

which has to satisfy the equation of induction and the boundary conditions on the perfect conductors at  $z = 0, 1$

$$\frac{\partial}{\partial t} \bar{B}_t = \mathcal{U}_\eta \frac{\partial^2}{\partial z^2} \bar{B}_t, \quad (4)$$

$$\frac{\partial}{\partial z} \bar{B}_t \Big|_{z=0} = \frac{\partial}{\partial z} \bar{B}_t \Big|_{z=1} = 0. \quad (5)$$

The time dependence of the reference magnetic field on the very slow diffusive timescale was introduced to allow for a non-trivial solution satisfying the boundary conditions (5), which would have to be spatially uniform for a stationary field. Because it is known (cf. Gilman 1970; Mizerski et al. 2013) that the magnetic buoyancy instability is excited only by magnetic fields that decrease with height, we take the solution

of Equation (4) in the following form

$$\bar{B}_t(z, t) = 1 + \frac{\Delta \bar{B}_t}{2} (e^{-\pi^2 \mathcal{U}_\eta t} \cos(\pi z) + 1), \quad (6)$$

where  $\Delta \bar{B}_t > 0$  is the nondimensional value of the magnetic field difference across the layer:  $\Delta \bar{B}_t = \bar{B}_t(0, t) - \bar{B}_t(1, t)$ . However, because the diffusion is very weak and the timescales of the instability are expected to be on the same order as the ideal case (i.e., proportional to the freefall timescale but much faster than the diffusive one), we can approximate the latter solution for times  $t \ll \mathcal{U}_\eta^{-1}$  to the following expression for stationary basic magnetic field  $\bar{B}(z)$  with only small corrections for diffusivity:

$$\bar{B}_t(z, t) \approx \bar{B}(z) = 1 + \frac{\Delta \bar{B}}{2} (\cos(\pi z) + 1). \quad (7)$$

In the following analysis, we use the basic magnetic field only in the time-independent form (7). The basic-state pressure  $\bar{p}(z)$  and density  $\bar{\rho}(z)$  are determined from the following equations:

$$0 = -\mathcal{P} \frac{d}{dz} \bar{p} - \frac{\Lambda}{2} \frac{d}{dz} \bar{B}^2 - \bar{\rho}, \quad (8)$$

$$\bar{p} = \alpha \bar{\rho}. \quad (9)$$

Thus, for the basic magnetic field given by (7), the density  $\bar{\rho}(z)$  has the following form

$$\begin{aligned} \bar{\rho}(z) = & \bar{\rho}(0) e^{-z/\mathcal{P}\alpha} + C_1 \sin(\pi z) \\ & + \pi C_1 \mathcal{P}\alpha (e^{-z/\mathcal{P}\alpha} - \cos(\pi z)) \\ & + C_2 \sin(2\pi z) + 2\pi C_2 \mathcal{P}\alpha (e^{-z/\mathcal{P}\alpha} - \cos(2\pi z)), \end{aligned} \quad (10)$$

where  $C_1 = (\pi \Lambda (\Delta \bar{B}/2) + \pi \Lambda (\Delta \bar{B}/2)^2) / (1 + (\pi \mathcal{P}\alpha)^2)$  and  $C_2 = \pi \Lambda (\Delta \bar{B}/2)^2 / (1 + (2\pi \mathcal{P}\alpha)^2)$ .

At this stage, we also define the following useful functions of the basic-state variables

$$\begin{aligned} H_\rho^{-1}(z) &= \bar{\rho}^{-1}(z) \frac{d}{dz} \bar{\rho}(z), \\ H_B^{-1}(z) &= \bar{B}^{-1}(z) \frac{d}{dz} \bar{B}(z), \end{aligned} \quad (11)$$

$$F(z) = \mathcal{P}\alpha + \frac{\Lambda \bar{B}^2(z)}{\bar{\rho}(z)} = \mathcal{P}\alpha (1 + \chi(z)), \quad (12)$$

where  $H_\rho^{-1}(z)$  and  $H_B^{-1}(z)$  are the depth-dependent inverse scale heights of density and magnetic field respectively, while  $F(z) = \mathcal{P}\alpha (1 + \chi(z))$  and  $\chi(z) = \Lambda \bar{B}^2(z) / (\mathcal{P}\alpha \bar{\rho}(z))$  are the same formulae as in Mizerski et al. (2013). The last two functions are always positive in the considered domain.

We note that the static-state Equations (8) and (9) also imply the following relation between those functions

$$H_\rho^{-1}(z) + \chi(z) H_B^{-1}(z) + (\mathcal{P}\alpha)^{-1} = 0. \quad (13)$$

In this section, just as Mizerski et al. (2013), we assume that the perturbations to the basic state have a form of interchange modes, i.e., they are assumed to be two-dimensional and varying in the  $y$  and  $z$  directions perpendicular to the basic

magnetic field

$$\begin{aligned} \mathbf{u} &= (0, v(z), w(z))e^{\sigma t +iky}, & \mathbf{b} &= (b_x(z), 0, 0)e^{\sigma t +iky}, \\ p &= \tilde{p}(z)e^{\sigma t +iky}, & \rho &= \tilde{\rho}(z)e^{\sigma t +iky}. \end{aligned} \quad (14)$$

Due to homogeneity in the  $y$  direction, a simple Fourier-mode type dependence is assumed, with the wavenumber denoted by  $k$  and the growth rate by  $\sigma$ . Later, in Section 6, we consider three-dimensional perturbations and derive the condition that has to be satisfied in order for the interchange modes to dominate.

Introduction of perturbations in the form (14) and the basic-state functions into Equations 1(a)–(f) and linearization yield the following system of linear equations

$$\sigma \tilde{\rho} i v = k(\mathcal{P}\tilde{p} + \Lambda \bar{B} b_x), \quad (15a)$$

$$\sigma \tilde{\rho} w = -\tilde{\rho} - \frac{d}{dz}(\mathcal{P}\tilde{p} + \Lambda \bar{B} b_x), \quad (15b)$$

$$\sigma b_x = -k \bar{B} i v - \frac{d}{dz}(\bar{B} w) + \mathcal{U}_\eta \frac{d^2}{dz^2} b_x - \mathcal{U}_\eta k^2 b_x, \quad (15c)$$

$$\sigma \tilde{\rho} = -k \tilde{\rho} i v - \frac{d}{dz}(\tilde{\rho} w), \quad (15d)$$

$$\tilde{p} = \alpha \tilde{\rho}. \quad (15e)$$

The top and bottom boundaries are assumed impermeable and (as already mentioned) perfectly conducting, which implies

$$\begin{aligned} w(z=0) &= w(z=1) = 0, \\ \frac{d}{dz} b_x \Big|_{z=0} &= \frac{d}{dz} b_x \Big|_{z=1} = 0. \end{aligned} \quad (16)$$

Due to the presence of the diffusive term in 15(c), the system of Equations 15(a)–(e) reduces (without any approximations) to one fourth-order ordinary differential equation for a chosen variable. We choose to express the stability problem in terms of a sole equation for the horizontal magnetic field perturbation  $b_x(z)$ , with the growth rate  $\sigma$  determined as the eigenvalue of the problem. The coefficients of this equation are very complicated and therefore cumbersome. However, we can express the equation in the simplified form

$$\begin{aligned} \tilde{f}_4(z) \frac{d^4}{dz^4} b_x(z) + \tilde{f}_3(z) \frac{d^3}{dz^3} b_x(z) + \tilde{f}_2(z) \frac{d^2}{dz^2} b_x(z) \\ + \tilde{f}_1(z) \frac{d}{dz} b_x(z) + \tilde{f}_0(z) b_x(z) = 0, \end{aligned} \quad (17)$$

where all the coefficients  $\tilde{f}_i(z)$ ,  $i = 0, \dots, 4$ , are dependent on the basic-state functions and their derivatives, the horizontal wavenumber  $k$ , the growth rate  $\sigma$ , and the dimensionless constants of the system, particularly  $\mathcal{U}_\eta$ . Their general form is provided in Appendix A.

In a general case, Equation (17) requires a numerical approach. We postpone the presentation of numerical results until Section 5. Following Gilman (1970), we first proceed by considering the short-wavelength asymptotic limit,  $k \gg 1$ , which is equivalent to the weak resistivity limit  $\mathcal{U}_\eta \ll 1$  in the analyzed case. The Rayleigh–Schrödinger analytic method utilized below for the asymptotic analysis is described in detail in Bender & Orszag (1978), and Mizerski et al. (2013) have applied it to the non-diffusive case.

All the details of the asymptotic analysis at the leading order can be found in Appendix A. Here, we describe only major

concepts and results. We assume that all the basic-state functions and their derivatives, the growth rate  $\sigma$ , and the dimensionless parameters except  $\mathcal{U}_\eta$  are on the order of unity. As argued by Gilman (1970), Acheson (1979), and Mizerski et al. (2013), the interchange modes become more unstable with growing wavenumbers, and without diffusion, the growth rate  $\sigma$  increases as  $k \rightarrow \infty$ . Thus, we expect that the effect of weak diffusion, which naturally tends to decrease the growth rate, will be simply to establish a finite magnitude of the large wavenumber  $k_{\max}$  for the most unstable mode; for  $k > k_{\max}$ , the diffusion is expected to continuously weaken the instability.

At this stage, it is useful to define an important function of the basic-state variables, denoted here by  $\sigma(z)$ , which appears in the leading-order analysis and will be called a “growth-rate function”

$$\sigma(z) = \sqrt{\frac{\Lambda \bar{B}^2(z)}{\tilde{\rho}(z) F(z)} (H_\rho^{-1}(z) - H_B^{-1}(z))}. \quad (18)$$

In the following, the function  $\sigma(z)$  always appears with an argument, whereas the symbol  $\sigma$  is retained to denote the true eigenvalue, which is a number. As demonstrated in Appendix A, the growth-rate function plays an important role in the analysis, because the most unstable mode localizes in the vicinity of the position of its maximum value in the domain, denoted by  $z_{\max}$ . Its value at that point,  $\sigma(z_{\max})$ , is equal to the growth rate of that most unstable mode at leading order, which we denote as  $\sigma_0$ . Thus,

$$\sigma_0 = \sigma(z_{\max}) = \sqrt{\frac{\Lambda \bar{B}^2(z_{\max})}{\tilde{\rho}(z_{\max}) F(z_{\max})} (H_\rho^{-1}(z_{\max}) - H_B^{-1}(z_{\max}))}, \quad (19)$$

and the situation is reminiscent of the non-diffusive case described in Mizerski et al. (2013), i.e., the most unstable eigenmode localizes in the vicinity of  $z_{\max}$ , where a boundary/internal layer is formed. In general, the modes can localize near the boundary (BL type modes, sometimes called “wall modes”) or inside the domain (internal-layer type, called “body modes”). We restrict our attention to body modes, but the results are easily generalizable to the case of wall modes (cf. Section 4.2. at Mizerski et al. 2013).

Additionally, we can also derive a criterion for instability (the same as in the non-diffusive case, cf. Acheson 1979 and Mizerski et al. 2013). The general condition  $\Re(\sigma) > 0$  leads to  $\Re(\sigma_0) > 0$ . Thus, from (19), we have

$$-H_B^{-1}(z_{\max}) > -H_\rho^{-1}(z_{\max}) > 0, \quad (20)$$

where the density scale height  $H_\rho$  is negative because we assume stable stratification. Therefore, the latter instability criterion demands also that the magnetic scale height  $H_B$  is negative, i.e., the horizontal magnetic field must decrease with height for the magnetic buoyancy instability to develop. By the use of relations (12) and (13), this criterion could be rewritten in the form

$$-H_B^{-1}(z_{\max}) > F^{-1}(z_{\max}) > 0. \quad (21)$$

Instability occurs when this criterion is satisfied at least locally, and the point  $z_{\max}$  is most prone to the instability.

As a result of further asymptotic analysis (see Appendix A for details), it occurs that the horizontal and vertical length

scales of variation of the most unstable perturbation are scaled with the fluid's resistivity as

$$k \sim \mathcal{U}_\eta^{-1/3}, \quad \delta \sim \mathcal{U}_\eta^{1/6}, \quad (22)$$

where  $\delta$  is the thickness of the boundary/internal layer of the mode, cf. Equation (55). An approximate expression for the growth rate of the most unstable mode takes the form (cf. Equation (74))

$$\begin{aligned} \sigma(k) = & \sigma_0 - \frac{1}{2\sqrt{2}} k^{-1} \sqrt{-\frac{d^2}{dz^2} \sigma^2(z) \Big|_{z=z_{\max}}} \\ & - \mathcal{U}_\eta k^2 \frac{\mathcal{P}\alpha}{2F(z_{\max})} + o(\mathcal{U}_\eta^{1/3}), \end{aligned} \quad (23)$$

and the leading-order form of the magnetic field perturbation is (cf. Equation (75))

$$b_{x,0}(z) = C \exp\left(-\frac{(z - z_{\max})^2}{2\sqrt{2}} k \sigma_0^{-1/2} \left(-\frac{d^2}{dz^2} \sigma^2(z) \Big|_{z=z_{\max}}\right)^{1/4}\right), \quad (24)$$

where  $C$  is an undetermined constant. The structure of the mode at the leading order is identical to the one in the case with no magnetic diffusion obtained in Mizerski et al. (2013), and the eigenmode is localized in the vicinity of the same  $z = z_{\max}$ . However, here we have established the order of the magnitude of the finite wavenumber of the most unstable mode, in terms of the weak resistivity, as  $k \sim \mathcal{U}_\eta^{-1/3}$ . The details of this analysis can be found in Appendix A.

At this stage, let us comment on the influence of the choice of boundary conditions in the analyzed problem. In the case of body modes (which localize away from the boundaries) such as (24), both the mode itself and its derivatives vanish at the boundaries. Nevertheless, even in this case, the boundary conditions are important when solving for the basic state, particularly the imposed magnetic field (cf. Equation (7)). In a diffusionless case, one can take a field linear in  $z$ , which one cannot do in the presence of diffusion, when the most reasonable and relatively simple boundary condition is to assume perfect conductors outside the domain. Moreover, the boundary conditions are important for the wall modes, i.e., the ones that localize near the boundaries; they are created when growth rate functions have their maximum values at the boundary. Those modes were studied in detail Mizerski et al. (2013). Because the approach in the case of wall modes is the same as for body modes, with the only notable difference being that their final structure is described by Airy instead of parabolic cylinder functions, we decided not to include them in the analysis presented here. Indeed, generalization of our analysis to wall modes is very straightforward. In the case of wall modes, the influence of the boundary conditions can be seen in the value of the correction to the growth rate at the order  $\delta^2$ , which differs depending on the choice of boundary conditions (perfect conductor versus insulator, no-slip versus stress-free). In each case, this correction is simply determined by either a zero of the Airy function or the derivative of the Airy function, but its order of magnitude remains the same, thus not violating the final conclusions.

#### 4. Joint Influence of Thermal and Magnetic Diffusivities

We will now consider the joint effect of the thermal and magnetic diffusivities—both are small, but the former is much greater than the latter—on the magnetic buoyancy instability in the short-wavelength limit. Therefore, we assume that the system is non-isothermal, and thus the energy Equation 1(c) is now coupled to the momentum, induction, and continuity equations through the equation of state. The thermal diffusion is characterized by the dimensionless thermal diffusivity parameter  $\mathcal{U}_\kappa \ll 1$ , which is assumed to be small. Such a regime is, in fact, opposite to the one considered in the previous section, where isothermal system was assumed, which is formally equivalent of the assumption  $\mathcal{U}_\kappa = \infty$ . On the other hand, it can be easily shown that the governing equations from this section can be reduced to those for the isothermal case by taking a limit  $\mathcal{U}_\kappa \rightarrow 0$  and  $\gamma \rightarrow 1$  with  $T = \text{const}$ . This is rather nonphysical, but convenient from a practical point of view because it is technically easy to apply and thus useful for comparison of the results obtained here with those from the previous section.

Guided by the parameter values for the solar tachocline provided in Gough (2007), which allow to estimate  $\mathcal{U}_\kappa \sim 10^{-10}$  and  $\mathcal{U}_\eta \sim 10^{-15}$ , we propose to study a regime described by the following power-law relation between the two diffusivities (see also Section 5 for numerical results)

$$\mathcal{U}_\eta \sim \mathcal{U}_\kappa^{3/2}, \quad (25)$$

which pertains to the tachocline. As in Section 3, we start by determining the basic state solution. Hence, in short, we consider a stationary layer of fluid in equilibrium, in dimensionless region  $0 \leq z \leq 1$ , with a horizontal, time-independent, and  $z$ -dependent magnetic field in the same form as in the previous section (cf. derivation of Equation (7)):

$$\vec{B} = \bar{B}(z) \hat{e}_x = \left(1 + \frac{\Delta \bar{B}}{2} (\cos(\pi z) + 1)\right) \hat{e}_x. \quad (26)$$

The basic-state pressure  $\bar{p}(z)$ , density  $\bar{\rho}(z)$ , and temperature  $\bar{T}(z)$  are now determined by the following set of equations

$$0 = -\mathcal{P} \frac{d}{dz} \bar{p} - \frac{\Lambda}{2} \frac{d}{dz} \bar{B}^2 - \bar{p}, \quad (27)$$

$$0 = \gamma \mathcal{U}_\kappa \frac{d^2}{dz^2} \bar{T} + \frac{(\gamma - 1)\Lambda}{\mathcal{P}\alpha} \mathcal{U}_\eta \left(\frac{d}{dz} \bar{B}\right)^2, \quad (28)$$

$$\bar{p} = \alpha \bar{\rho} \bar{T}. \quad (29)$$

Thus, from Equation (28) and for the basic magnetic field given by (26), the basic-state temperature  $\bar{T}$  has the following form

$$\begin{aligned} \bar{T}(z) = & 1 + \Delta \bar{T} (1 - z) - \theta (z^2 - z) \\ & + \frac{\theta}{2\pi^2} (1 - \cos(2\pi z)), \end{aligned} \quad (30)$$

where  $\theta = (\gamma - 1)(\lambda/2)^2 \pi^2 \Lambda \mathcal{U}_\eta / (4\mathcal{P}\alpha\gamma\mathcal{U}_\kappa) > 0$  and  $\Delta \bar{T} > 0$  is the nondimensional temperature jump across the layer,  $\Delta \bar{T} = \bar{T}(0) - \bar{T}(1)$ . For the temperature given by the formula (30), the basic-state density  $\bar{\rho}$  can only be found numerically from Equations (27) and (29). However, it is worth noting that, with relation (25), parameter  $\theta$  becomes of the order  $\mathcal{U}_\kappa^{1/2} \ll 1$ , and thus the basic-state temperature  $\bar{T}$  is approximately linear in  $z$  with a negative gradient of  $-\Delta \bar{T}$ .

At this stage, it is useful to define the following functions of the basic-state variables

$$\begin{aligned} H_T^{-1}(z) &= \bar{T}^{-1}(z) \frac{d}{dz} \bar{T}(z), \\ F_\gamma(z) &= \mathcal{P} \alpha \bar{T}(z) \gamma + \frac{\Lambda \bar{B}^2(z)}{\bar{\rho}(z)} = \mathcal{P} \alpha \bar{T}(z) \gamma (1 + \chi_\gamma(z)), \end{aligned} \quad (31)$$

where  $H_T^{-1}$  is a depth-dependent inverse scale height of the temperature, while  $\chi_\gamma(z) = \Lambda \bar{B}^2(z) / (\mathcal{P} \alpha \bar{T}(z) \gamma \bar{\rho}(z))$  (cf. similar definitions in (12) for the isothermal case). The functions  $F_\gamma(z)$  and  $\chi_\gamma(z)$  are always positive in our domain. In the following, we will also use functions  $F(z)$  and  $\chi(z)$  defined similarly as in (12), but in a non-isothermal form that takes into account the basic temperature dependence of the system. In other words, we now replace parameter  $\alpha$ , in the form utilized in previous sections, with the term  $\alpha \bar{T}(z)$ :

$$\begin{aligned} F(z) &= \mathcal{P} \alpha \bar{T}(z) + \Lambda \bar{B}^2(z) / \bar{\rho}(z), \\ \chi(z) &= \Lambda \bar{B}^2(z) / (\mathcal{P} \alpha \bar{T}(z) \bar{\rho}(z)). \end{aligned} \quad (32)$$

From Equations (27) and (29), one can derive the following useful relation for the scale heights

$$H_T^{-1}(z) + H_\rho^{-1}(z) + \chi(z) H_B^{-1}(z) + (\mathcal{P} \alpha \bar{T}(z))^{-1} = 0. \quad (33)$$

In this case, we also assume at the first stage that the perturbations to the basic state have the following form of interchange modes: two-dimensional and varying in the  $y$  and  $z$  directions, perpendicular to the basic magnetic field. Their wavenumber in the  $y$  direction is denoted by  $k$  and the growth rate by  $\sigma$ . The more general case of three-dimensional modes is presented in Section 6. Two-dimensional perturbations adopt the following form

$$\mathbf{u} = (0, v(z), w(z)) e^{\sigma t + iky}, \quad \mathbf{b} = (b_x(z), 0, 0) e^{\sigma t + iky}, \quad (34a)$$

$$\begin{aligned} p &= \bar{p}(z) e^{\sigma t + iky}, & \rho &= \bar{\rho}(z) e^{\sigma t + iky}, \\ T &= \bar{T}(z) e^{\sigma t + iky}. \end{aligned} \quad (34b)$$

Introducing 34(a) and (b) into Equations 1(a)–(e) and linearizing, we obtain the following set of equations

$$\sigma \bar{\rho} v = -ik(\mathcal{P} \bar{p} + \Lambda \bar{B} b_x), \quad (35a)$$

$$\sigma \bar{\rho} w = -\bar{\rho} - \frac{d}{dz}(\mathcal{P} \bar{p} + \Lambda \bar{B} b_x), \quad (35b)$$

$$\sigma b_x = -ik \bar{B} v - \frac{d}{dz}(\bar{B} w) + \mathcal{U}_\eta \frac{d^2}{dz^2} b_x - \mathcal{U}_\eta k^2 b_x, \quad (35c)$$

$$\begin{aligned} \sigma \bar{\rho} \bar{T} &= -\bar{\rho} \bar{T}' w + \gamma \mathcal{U}_\kappa \frac{d^2}{dz^2} \bar{T} - \gamma \mathcal{U}_\kappa k^2 \bar{T} - \frac{\gamma - 1}{\alpha} ik \bar{p} v \\ &\quad - \frac{\gamma - 1}{\alpha} \bar{p} \frac{d}{dz} w + \frac{2(\gamma - 1)\Lambda}{\mathcal{P} \alpha} \mathcal{U}_\eta \bar{B}' \frac{d}{dz} b_x, \end{aligned} \quad (35d)$$

$$\sigma \bar{p} = -ik \bar{\rho} v - \frac{d}{dz}(\bar{\rho} w), \quad (35e)$$

$$\bar{p} = \alpha \bar{\rho} \bar{T} + \alpha \bar{T} \bar{p}. \quad (35f)$$

The boundaries are assumed impermeable, perfectly conducting, and isothermal; for the perturbation fields, this yields:

$$\begin{aligned} w(z=0) &= w(z=1) = 0, \\ \frac{d}{dz} b_x \Big|_{z=0} &= \frac{d}{dz} b_x \Big|_{z=1} = 0, \\ \bar{T}(z=0) &= \bar{T}(z=1) = 0. \end{aligned} \quad (36)$$

By manipulating Equations 35(a)–(f), one could formally obtain a single sixth-order differential equation for the vertical velocity  $w(z)$ . However, such an equation has extremely cumbersome coefficients, which makes the analysis very difficult. Thus, in the current case, we adopt the following approach. First, guided by the previously obtained results in Section 3 and Mizerski et al. (2013), we derive scaling relations for the magnitudes of perturbation fields  $w(z)$ ,  $v(z)$ ,  $b_x(z)$ ,  $\bar{p}(z)$ ,  $\bar{\rho}(z)$ ,  $\bar{T}(z)$  for the most unstable mode. These scalings, expressed in terms of the large wavenumber, turn out to be the same in both already resolved problems, i.e., the non-diffusive case analyzed in Mizerski et al. (2013) and the isothermal case with non-zero magnetic diffusion from the previous section. We then speculate that these scalings persist also when the temperature variations are allowed, and we apply them to the Equations 35(a)–(f). Consequently, one second-order ordinary differential equation for the vertical velocity perturbation  $w(z)$  can be obtained at the leading order. This equation is then analyzed to obtain the structure of the most unstable mode, its growth rate, and the magnitude of the wavenumber in terms of the diffusion parameters  $\mathcal{U}_\kappa$  and  $\mathcal{U}_\eta$ . This approach and its results were validated by the numerical simulations of the full system of perturbation (Equations 35(a)–(f)) presented in Section 5.

As remarked previously, the aforementioned scaling relations are obtained from careful consideration of the linear equations for perturbations 15(a)–(e) in the previous isothermal case. The derivation of Equation (73) and analogous Equation 33(c) in Mizerski et al. (2013), which both describe the strongly localized, most unstable mode, can be traced back to the set of original linear equations 15(a)–(e) (and (14)–(18) in Mizerski et al. 2013) for all perturbation fields, which allow to express the magnitudes of  $v(z)$ ,  $b_x(z)$ ,  $\bar{p}(z)$ , and  $\bar{\rho}(z)$  via the magnitude of the vertical velocity  $w(z)$  in the following way

$$\begin{aligned} \bar{\rho}(z) &\sim \bar{p}(z) \sim b_x(z) \sim w(z), & v(z) &\sim k^{-1/2} w(z), \\ \pi(z) &\sim k^{-3/2} w(z), \end{aligned} \quad (37)$$

where  $\pi(z) = \mathcal{P} \bar{p}(z) + \Lambda \bar{B} b_x(z)$  is the total pressure. The scalings (37) introduced into the Equations 35(a)–(f) imply only one consistent relation between the scale of the temperature perturbation function  $\bar{T}(z)$  and  $w(z)$ , namely

$$\bar{T}(z) \sim w(z). \quad (38)$$

Application of (37) and (38) to the set of perturbation Equations 35(a)–(f) allows to transform this set into one sixth-order ordinary differential equation, which (in a local variable) becomes second-order at the leading order. The detailed analysis of this Equation (80) is provided in Appendix B. Here, we present only the results and conclusions.

At this stage, we introduce the following notation for three basic-state dependent functions ( $z$ -dependent only), which can

be thought of as three independent growth-rate functions:

$$\sigma(z) = \sqrt{\frac{\Lambda \bar{B}^2(z)}{\bar{\rho}(z)F(z)}(H_\rho^{-1}(z) - H_B^{-1}(z))}, \quad (39)$$

$$\sigma_T(z) = \sqrt{\frac{\Lambda \bar{B}^2(z)}{\bar{\rho}(z)F_\gamma(z)}(H_\rho^{-1}(z) - H_B^{-1}(z)) + \frac{\mathcal{P}\alpha\bar{T}(z)(\gamma - 1)}{F_\gamma(z)}\left(H_\rho^{-1}(z) - \frac{H_T^{-1}(z)}{(\gamma - 1)}\right)}, \quad (40)$$

$$\sigma_{4/3}(z) = \sqrt{\sigma^2(z) + \left(\frac{\mathcal{U}_\eta k^2 \mathcal{P}\alpha\bar{T}(z)}{2F(z)}\right)^2} - \frac{\mathcal{U}_\eta k^2 \mathcal{P}\alpha\bar{T}(z)}{2F(z)}. \quad (41)$$

The function  $\sigma(z)$  is similar to (18), but it takes into account the non-uniform basic-state temperature profile in  $F(z)$  and the new form of  $\bar{\rho}(z)$ . The functions  $\sigma_T(z)$  and  $\sigma_{4/3}(z)$  are the new growth-rate functions, which have no analog in the isothermal case. They all play an important role in the asymptotic analysis, and each of them provides a dominant contribution to the growth rate in different physical regimes. As demonstrated in Appendix B, the most unstable mode localizes in the vicinity of the position of maximum value of one of the above growth-rate functions in the domain, denoted by  $z_{0,\max}$ ,  $z_{T,\max}$ , or  $z_{\max}$ , respectively, where the value of the corresponding growth-rate function at that point  $\sigma(z_{0,\max})$ ,  $\sigma_T(z_{T,\max})$  or  $\sigma_{4/3}(z_{\max})$  is equal to the growth rate  $\sigma_0$  of the most unstable mode at the leading order.

Although it is not a trivial task to determine which of the growth-rate functions describes the most unstable mode, some general relations between those growth rate functions can be obtained relatively easily. First, it is straightforward to see that, for all  $0 \leq z \leq 1$ , we have  $\sigma(z) > \sigma_{4/3}(z)$ . Furthermore, a criterion for dominance of functions (39) and (40) can also be found (cf. Equation (83) and the following comment)

$$-H_T^{-1} > \frac{(\gamma - 1)}{F_\gamma} \iff \sigma_T(z) > \sigma(z). \quad (42)$$

We are now ready to summarize the results obtained via the asymptotic analysis—presented in detail in Appendix B—and speculate about their possible applications to the solar tachocline. When both diffusivities are non-zero and related through  $\mathcal{U}_\eta \sim \mathcal{U}_\kappa^{3/2} \ll 1$ , the following distinct regimes can be identified.

1. When the basic-state solution satisfies  $\sigma(z_{0,\max}) > \sigma_T(z_{T,\max})$  there are three possibilities:

(i) The wavenumber  $k$  is not large enough for the full asymptotics to set in, and therefore the most unstable mode chosen by the system is described by  $\sigma_0 = \sigma(z_{0,\max})$  and  $k \sim \mathcal{U}_\kappa^{-3/5}$  (together with  $\delta \sim k^{-1/2} \sim \mathcal{U}_\kappa^{3/10}$  and  $\sigma = \sigma_0 + k^{-1/2}\sigma_1 + k^{-1}\sigma_2 + \dots$ ). This solution, which we named a “partly asymptotic solution,” was the only one that emerged in the numerical simulations of this regime. It corresponds to diffusivities as low as  $\mathcal{U}_\kappa = 10^{-8}$  (and possibly even lower, because the main requirement for this solution to set in is that  $\sigma(z_{0,\max})(\sigma^2(z_{0,\max}) - \sigma_T^2(z_{0,\max})) \sim \mathcal{U}_\kappa^{1/10}$ ,

which for  $\mathcal{U}_\kappa = 10^{-8}$  ( $k \sim 5.5 \times 10^4$ ) gives  $\mathcal{U}_\kappa^{1/10} \approx 0.16$ , whereas for  $\mathcal{U}_\kappa = 10^{-10}$  ( $k \sim 10^6$ ) two orders of magnitude lower ( $k$  about 20 times larger) gives a very similar value  $\mathcal{U}_\kappa^{1/10} = 0.1$ ). By the use of the numerical values of physical parameters obtained for the solar tachocline from observations and provided by Gough (2007), we can estimate the diffusivities at  $\mathcal{U}_\kappa \sim 10^{-10}$  and  $\mathcal{U}_\eta \sim 10^{-15}$ , which allows to provide an estimate for the short-wavelength of the most unstable mode  $\lambda_{\max} = 2\pi/k \sim 2\pi d \mathcal{U}_\kappa^{3/5} \approx 220$  m, where  $d \approx 3.5 \times 10^7$  m is the tachocline thickness. An estimate of waves as short as hundreds of meters in the tachocline seems rather short, although it must be remembered that it utilizes only the order of magnitude of the wavenumber. Thus, if  $k \sim 0.2 \times \mathcal{U}_\kappa^{-3/5}$  for example, this would lead to wavelengths of the most unstable mode at the order of a kilometer. Whether such short waves can exist in the tachocline is not clear at this stage.

(ii) The second possibility is that the system reaches the final asymptotic limit, but a more restrictive condition than  $\sigma(z_{0,\max}) > \sigma_T(z_{T,\max})$  is satisfied, i.e.,  $\sigma_{4/3}(z_{\max}) > \sigma_T(z_{T,\max})$ . In such a regime, the most unstable mode is described by  $\sigma_0 = \sigma_{4/3}(z_{\max}) < \sigma(z_{0,\max})$ ,  $k \sim \mathcal{U}_\kappa^{-3/4}$ ,  $\delta \sim k^{-1/2} \sim \mathcal{U}_\kappa^{3/8}$ , and  $\sigma = \sigma_0 + k^{-2/3}\sigma_1 + k^{-1}\sigma_2 + \dots$ . An estimate of the wavelength of the most unstable mode corresponding to the solar tachocline conditions leads to nonphysically short waves with  $\lambda_{\max}$  at the order of meters.

(iii) The last possibility is also obtained in a fully asymptotic regime, but under conditions corresponding to  $\sigma_{4/3}(z_{\max}) < \sigma_T(z_{T,\max}) < \sigma(z_{0,\max})$ , which leads to  $\sigma_0 = \sigma_T(z_{T,\max})$ ,  $k \sim \mathcal{U}_\kappa^{-1/3}$ ,  $\delta \sim k^{-1/2} \sim \mathcal{U}_\kappa^{1/6}$ , and  $\sigma = \sigma_0 + k^{-1}\sigma_2 + \dots$  for the most unstable mode. In the context of the solar tachocline, this regime corresponds to the most unstable modes with a wavelength of  $\lambda_{\max} \approx 10^2$  km, which seems reasonable for the tachocline.

2. In the opposite regime, characterized by  $\sigma(z_{0,\max}) < \sigma_T(z_{T,\max})$ , the most unstable mode is always the one described in the last case (iii) of point 1, i.e.,  $\sigma_0 = \sigma_T(z_{T,\max})$ ,  $k \sim \mathcal{U}_\kappa^{-1/3}$ ,  $\delta \sim k^{-1/2} \sim \mathcal{U}_\kappa^{1/6}$ , and  $\sigma = \sigma_0 + k^{-1}\sigma_2 + \dots$ , which corresponds to  $\lambda_{\max} \approx 10^2$  km in the parameter regime corresponding to that of the tachocline.

Approximate expressions for the growth rates of the most unstable modes and the leading-order form of the vertical velocity perturbation for the described regimes can be found in Appendix B. In the case of regimes (1)(iii) and (2), strongly influenced by thermal effects, the instability criterion differs from the simple  $-H_B^{-1} > 0$  (cf. Equation (20)) and takes the form

$$-H_B^{-1}(z_0) - \chi^{-1}(z_0)H_T^{-1}(z_0) > F_\gamma^{-1}(z_0)(1 + (\gamma - 1)\chi^{-1}(z_0)) > 0. \quad (43)$$

It can be seen that, essentially, there are only two fully asymptotic regimes, i.e., when  $\sigma_{4/3}(z_{\max}) > \sigma_T(z_{T,\max})$ , we get the mode  $\sigma \approx \sigma_{4/3}(z_{\max})$  and  $k \sim \mathcal{U}_\kappa^{-3/4}$ ; in the opposite case of  $\sigma_{4/3}(z_{\max}) < \sigma_T(z_{T,\max})$ , the dominant mode is characterized

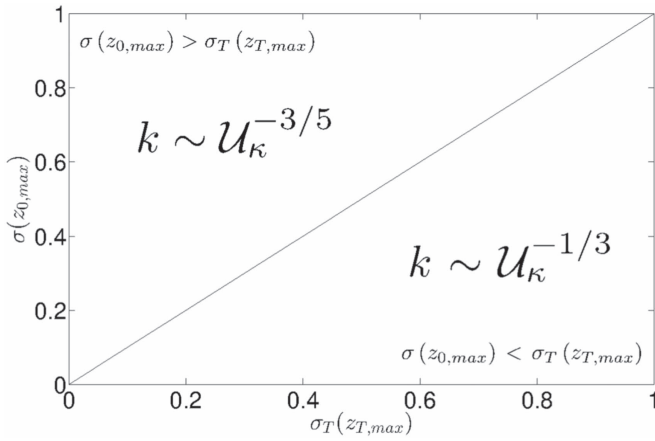


**Figure 1.** The schematic diagram shows the most unstable mode wavenumber  $k$  scaled by the thermal diffusivity parameter  $\mathcal{U}_\kappa$  in a dependence from the relation between the maxima of growth-rate functions  $\sigma(z)$  and  $\sigma_T(z)$ .

by  $\sigma \approx \sigma_T(z_{T,\max})$  and  $k \sim \mathcal{U}_\kappa^{-1/3}$ . However, there is also a partly asymptotic solution, which dominates when  $\sigma(z_{0,\max}) > \sigma_T(z_{T,\max})$  (requiring also  $\sigma(z_{0,\max})(\sigma^2(z_{0,\max}) - \sigma_T^2(z_{0,\max})) \sim \mathcal{U}_\kappa^{1/10}$ ), which is still achieved for very small diffusivities (as small as  $\mathcal{U}_\kappa = 10^{-8}$  in the full numerical solutions) and large wavenumbers (as high as  $k \sim 5.5 \times 10^4$ ), corresponding to  $\sigma \approx \sigma(z_{0,\max})$  and  $k \sim \mathcal{U}_\kappa^{-3/5}$  for the most unstable mode.

When relating the obtained results to the solar tachocline, in order to obtain a rough picture of the true dynamics, it could be reasonable to start by elimination of very short waves, e.g., with wavelengths at the order of meters, due to the large length scales of the entire domain: a vertical span of  $10^7$  m and axial of  $10^9$  m at the equator. Such short waves would correspond to very high azimuthal wavenumbers and therefore are expected to be initially very weak. Moreover, the unstable waves are localized in the vertical direction; therefore, those with very short wavelengths appear only in a very short vertical region. In that spirit, the final conclusion depends on where we put such a geometrical bound, but it is of some interest to observe, that, e.g., if we expect  $k \lesssim 10^4$  ( $\lambda \gtrsim 2 \times 10^4$  m), only the two cases corresponding to  $\sigma \approx \sigma(z_{0,\max})$  with  $k \sim \mathcal{U}_\kappa^{-3/5}$  or  $\sigma \approx \sigma_T(z_{T,\max})$  with  $k \sim \mathcal{U}_\kappa^{-1/3}$  can be dynamically relevant (however, in principle, it must be remembered that there is no clear criterion that would allow to neglect the global dynamical influence of very short waves with respect to that of longer waves). Figure 1 presents a schematic diagram of the two (in our opinion) most physically relevant dynamical regimes among those described above, namely regimes described in points (1)(i) and (2). The two distinct regimes determined by the relation between system parameters and basic-state profiles contained in the growth-rate functions  $\sigma(z_{0,\max})$  and  $\sigma_T(z_{T,\max})$  and the scalings for the wavenumber  $k$  of the most unstable mode with the thermal diffusivity parameter  $\mathcal{U}_\kappa$  for each of the dynamical regimes are clearly shown.

As remarked in the introduction, our analysis is deprived of the vital influence of shear (to be included in future studies). Hence, the discussion related to the tachocline is rather speculative at this stage. However, on a final note, we would like to comment on the relation (42). Namely, we speculate which of the identified regimes could be expected in the

tachocline. In order to do that, we must estimate the magnitude of the temperature scale height in the tachocline, which we achieve by the use of pressure ( $H_p$ ) and density ( $H_\rho$ ) scale heights estimates at the bottom of the solar convection zone provided by Gough (2007) and the relation  $-H_T^{-1} = H_p^{-1} - H_\rho^{-1}$  satisfied by an ideal gas. This leads to  $-H_T^{-1} \approx 0.2$  in units of the tachocline thickness  $d \approx 3.5 \times 10^7$  m. The solar tachocline parameters given in Gough (2007) allow to estimate also the right-hand side of (42) at the bottom of the convection zone, which yields  $(\gamma - 1)/F_\gamma \approx (\gamma - 1)/\gamma \approx 0.4$  for  $\gamma = 1.665$ . The estimates reveal that  $(\gamma - 1)/F_\gamma$  is about twice the inverse temperature scale height, which could suggest, according to inequality (42), that the tachocline, at least in the upper parts, falls into the regime  $\sigma(z_{0,\max}) > \sigma_T(z_{T,\max})$  (1i above) with the most unstable mode described by  $\sigma_0 = \sigma(z_{0,\max})$  and  $k \sim \mathcal{U}_\kappa^{-3/5}$ . However, with the current uncertainty of the physical parameter values for the solar tachocline, the factor of two appearing in the inequality (42) does not seem convincing enough to determine which dynamical regime the tachocline is in.

## 5. Numerical Simulations

In Sections 3 and 4, we presented the results of a linear analysis of two-dimensional magnetic buoyancy instability in the form of an eigenvalue problem for the systems of Equations 15(a)–(e) and 35(a)–(f). Here we present the numerical solutions of the both equation sets. The equations were discretized using a standard second order finite difference method and for the so-obtained matrices on the right-hand sides of those equations the eigenvalues  $\sigma$  with the greatest positive real parts (to find the most unstable modes) in each spectrum corresponding to different values of the wavenumber and the associated eigenfunctions were computed with the use of standard MATLAB procedures. Since the modes are assumed 2D and in the form 34(b), one needs to maximize the eigenvalue  $\sigma$  over all possible wavenumbers  $k \in (0, \infty)$ , for a fixed set of nondimensional parameters of the system, in particular the magnetic diffusivity  $\mathcal{U}_\eta$  and thermal diffusivity  $\mathcal{U}_\kappa$ . Naturally in the numerical computations only a finite set of the wavenumbers was used, however the results seem to clearly indicate, that the obtained maxima of the  $\sigma(k)$  dependence are global.

### 5.1. The Effect of Magnetic Diffusivity

We present the results of numerical analysis of the isothermal case in the presence of asymptotically small magnetic diffusivity  $\mathcal{U}_\eta$  (cf. Section 3). We focus on the case when the maximum of the so-called growth rate function  $\sigma(z)$  defined in (18) is strictly inside the domain. The applied boundary conditions are in the form of (16), i.e., we impose impermeability for the vertical velocity and perfect conductors outside the domain for the magnetic field, and the external magnetic field is given by (7). Because we account for the perfectly conducting boundaries, the basic magnetic field differs from that assumed in the isothermal diffusionless case analyzed in Mizerski et al. (2013). Despite that, for the sake of correspondence, we choose here the same parameter values as in “Case 1” of Section 5 in Mizerski et al. (2013):  $\alpha = 1.00$ ,  $\Lambda = 0.20$ ,  $\Delta\bar{B} = 1.35$ ,  $\mathcal{P} = 1.90$ ,  $\bar{\rho}(z=0) = 1.39$ . For this



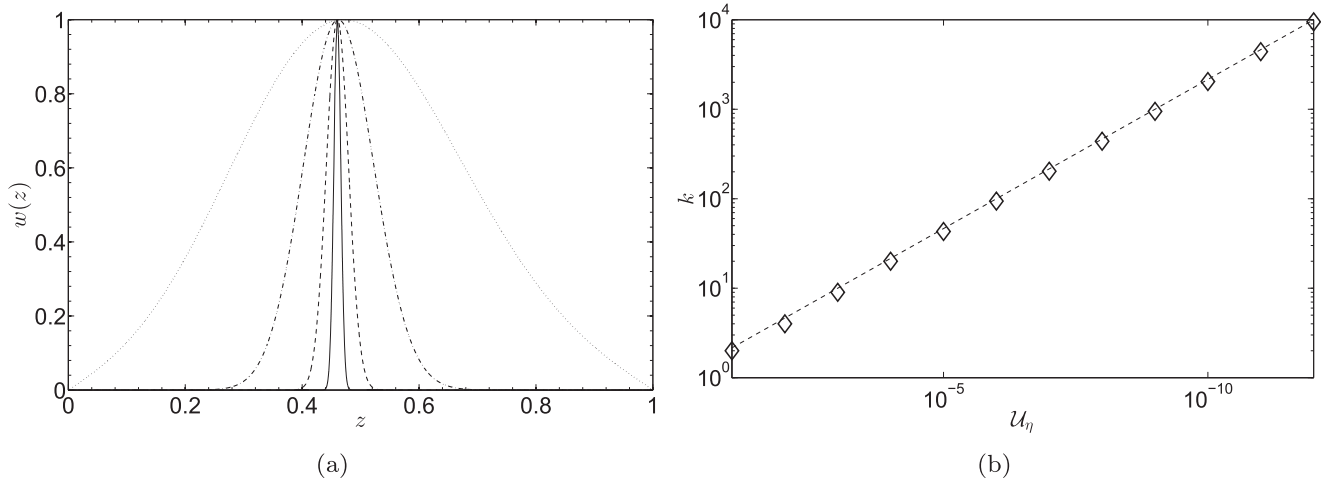


**Figure 2.** (a) Vertical velocity  $w(z)$  of the most unstable modes for:  $\mathcal{U}_\eta = 10^{-3}$  ( $k = 9$ ,  $\sigma = 0.35591$ ; dotted line),  $\mathcal{U}_\eta = 10^{-6}$  ( $k = 94$ ,  $\sigma = 0.44846$ ; dotted-dashed line),  $\mathcal{U}_\eta = 10^{-9}$  ( $k = 947$ ,  $\sigma = 0.45797$ ; dashed line),  $\mathcal{U}_\eta = 10^{-12}$  ( $k = 9477$ ,  $\sigma = 0.45892$ ; solid line). Other parameters values:  $\alpha = 1.00$ ,  $\Lambda = 0.20$ ,  $\Delta\bar{B} = 1.35$ ,  $\mathcal{P} = 1.90$ ,  $\bar{p}(z=0) = 1.39$ . (b) Relation between the wavenumber  $k$  and magnetic diffusivity  $\mathcal{U}_\eta$ . Numerical results are depicted as diamonds, and the analytic relation  $k = \mathcal{U}_\eta^{-1/3}$  is shown as a dashed line.

set of parameters, the maximum of the function  $\sigma(z)$  is now equal to  $\sigma_{\max} = 0.45903$  and is achieved at  $z_{\max} = 0.4602$ .

Four different values of the magnetic diffusivity  $\mathcal{U}_\eta = 10^{-3}$ ,  $10^{-6}$ ,  $10^{-9}$ ,  $10^{-12}$  were studied. For each case, we found the growth rate  $\sigma$  and the wavenumber  $k$  of the most unstable mode, as well as its structure. The vertical velocity  $w(z)$  for the most unstable modes is depicted in Figure 2(a) for all four values of  $\mathcal{U}_\eta$ , with the values of the adequate growth rates and wavenumbers given in the caption. It can be seen that, for all values of  $\mathcal{U}_\eta$  between  $10^{-3}$  and  $10^{-12}$ , the maximum of the most unstable mode is located near the same point  $z_0 \approx 0.46$ , almost equal to the theoretical value of  $z_{\max}$ , which is consistent with the predictions and the results from Section 3, especially the form of the mode given by the formula (24). However, with decreasing magnetic diffusivity, the wavenumber  $k$  of the most unstable mode increases, and thus the mode becomes more localized. A relation (22) between the wavenumber and magnetic diffusivity found at the end of Section 3 for the most unstable mode is confirmed numerically, as Figure 2(b) demonstrates, establishing the proportionality coefficient,  $k \approx 0.95 \mathcal{U}_\eta^{-1/3}$ , for the asymptotic regime  $\mathcal{U}_\eta \rightarrow 0$ . Moreover, the presence of the magnetic diffusivity affects the growth rate of the most unstable mode, which is getting closer to the theoretical value of  $\sigma_{\max}$  when  $\mathcal{U}_\eta$  tends to zero. This is consistent with the asymptotic form of the growth rate given by the formula (23).

In Figure 3, we show the relation between the growth rate  $\sigma$  and the wavenumber  $k$  for magnetic diffusivity  $\mathcal{U}_\eta = 10^{-9}$  (a “dispersion relation”). The dots are the highest values of the growth rate obtained for a specific value of  $k$  from numerical solutions. The horizontal dashed line corresponds to the theoretical value of the maximal growth rate at the leading order,  $\sigma_{\max} = 0.45903$ . The most unstable mode for this value of  $\mathcal{U}_\eta$  has a wavenumber  $k = 947$ , with growth rate  $\sigma = 0.45797$ . All modes with greater wavenumbers have a smaller growth rate, which tends to zero at fixed  $\mathcal{U}_\eta$  when  $k \rightarrow \infty$ . This clearly shows the effect of magnetic diffusivity on the short-wavelength modes; namely, to establish a finite magnitude of the wavenumber of the most unstable mode through dominance of the diffusive decay at large enough

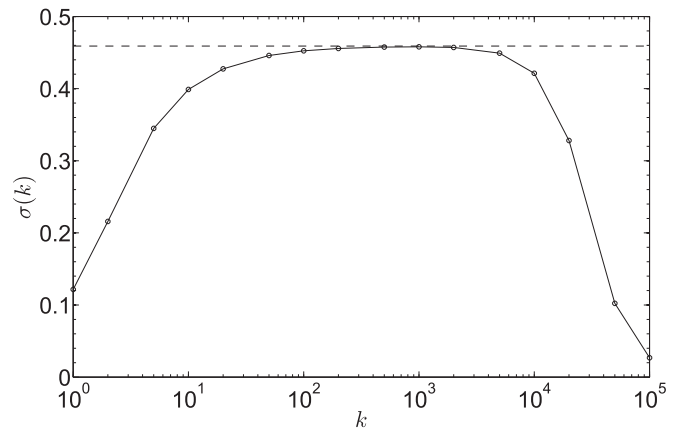


**Figure 3.** The relation between the numerically found growth rate  $\sigma$  and the wavenumber  $k$  for magnetic diffusivity  $\mathcal{U}_\eta = 10^{-9}$  and  $\mathcal{U}_\kappa = \infty$  (dots connected by a solid line); analytically found growth rate at the leading order,  $\sigma_0$  (dashed line). Other parameter values as in Figure 2.

wavenumbers, unlike in the case without dissipation, when growth rate approaches its maximal value in the limit  $k \rightarrow \infty$ .

## 5.2. The Effect of Thermal Diffusivity

We now turn to the numerical analysis of the case with values for both diffusivities, thermal  $\mathcal{U}_\kappa$  and magnetic  $\mathcal{U}_\eta$ , that are non-zero but asymptotically small, related through (25), namely  $\mathcal{U}_\eta \sim \mathcal{U}_\kappa^{3/2}$ , which was analytically resolved in Section 4. This case is non-isothermal and the basic-state temperature is given by (30). The analysis of Section 4 has provided us with knowledge of three functions  $\sigma(z)$  (39),  $\sigma_T(z)$  (40), and  $\sigma_{4/3}(z)$  (41), whose maximum values determine the growth rate and the region of localization of the most unstable modes in different regimes. However, out of four different theoretically discovered possibilities, only two regimes corresponding to either  $\sigma(z_{0,\max}) > \sigma_T(z_{T,\max})$  or  $\sigma(z_{0,\max}) < \sigma_T(z_{T,\max})$  are manifested in the numerical solutions, because the other two cases require numerically unachievable small diffusivities. The boundary conditions for perturbations are given by formula (36). For the sake of clear comparison, we choose here the same values of the physical parameters

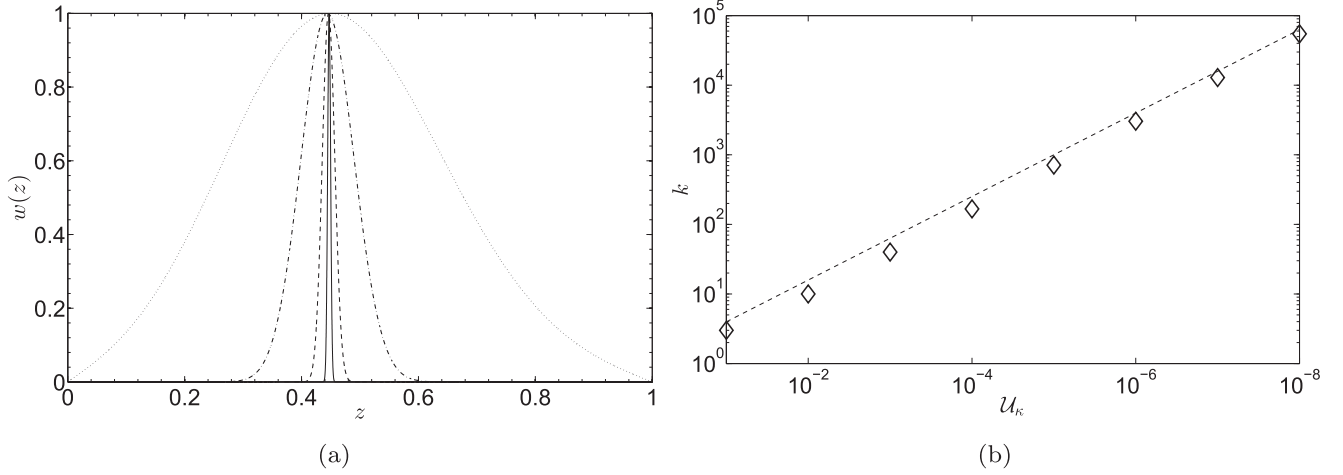


**Figure 4.** (a) Vertical velocity  $w(z)$  for the most unstable modes for  $\Delta\bar{T} = 0.1$ , and:  $U_\kappa = 10^{-2}$  and  $U_\eta = 10^{-3}$  ( $k = 10$ ,  $\sigma = 0.33844$ ; solid line),  $U_\kappa = 10^{-4}$  and  $U_\eta = 10^{-6}$  ( $k = 167$ ,  $\sigma = 0.43494$ ; dashed line),  $U_\kappa = 10^{-6}$  and  $U_\eta = 10^{-9}$  ( $k = 3033$ ,  $\sigma = 0.45292$ ; dotted-dashed line),  $U_\kappa = 10^{-8}$  and  $U_\eta = 10^{-12}$  ( $k = 54668$ ,  $\sigma = 0.45813$ ; dotted line). Other parameter values as on Figure 2; (b) relation between the wavenumber  $k$  and thermal diffusivity  $U_\kappa$ : numerical results (diamonds) and analytic relation  $k = U_\kappa^{-3/5}$  (dashed line).  $\Delta\bar{T} = 0.1$ , other parameters values as on Figure 2.

as in the section above:  $\alpha = 1.00$ ,  $\Lambda = 0.20$ ,  $\Delta\bar{B} = 1.35$ ,  $\mathcal{P} = 1.90$ ,  $\bar{\rho}(z=0) = 1.39$ . Diffusivity parameters are related through (25) in all the simulations.

The temperature jump across a layer  $\Delta\bar{T}$ , given in (30), plays an important role in the dynamics. According to (83) when  $\Delta\bar{T}$  is greater than some critical value  $\Delta\bar{T}_{c1}$ , the function  $\sigma_T(z)$  will always have a maximum value greater than the maximum value of the function  $\sigma(z)$ . Hence in such case the growth rate and the point of localization of the most unstable mode is determined by the former function, which in turn results in a distinguished limit, which establishes the order of magnitude of the wavenumber and the mode structure, as demonstrated in Section 4. For the assumed set of parameter values we get  $\Delta\bar{T}_{c1} \approx 0.18$ , which slightly depends on the values of the diffusivities. Furthermore, other critical value  $\Delta\bar{T}_{c2}$  determines whether or not our basic state density is monotonically decreasing with increasing  $z$ , which is a physical requirement imposed on the basic state solution. For the mentioned parameter values  $\Delta\bar{T}_{c2} \approx 0.23$  which means, that for stronger temperature jumps across the layer,  $\Delta\bar{T} > 0.23$  the density profile becomes unstable with a heavier fluid on top of the lighter and the Rayleigh–Taylor instability enters the dynamics. Such a situation is undesirable and we exclude it by taking the temperature jumps  $\Delta\bar{T} < \Delta\bar{T}_{c2} \approx 0.23$ . This corresponds to what we expect for the tachocline which is believed to have a stable density stratification.

Figure 4 presents the vertical velocity  $w(z)$  and the  $k(U_\kappa)$  dependence for the most unstable modes for different values of the thermal and magnetic diffusivities and for  $\Delta\bar{T} = 0.1 < \Delta\bar{T}_{c1}$ , so that  $\sigma(z_{0,\max}) > \sigma_T(z_{T,\max})$ . In this case the growth rate functions have the following maximum values:  $\sigma(z_{0,\max} = 0.44880) = 0.46043$  and  $\sigma_{T,\max}(z_{T,\max} = 0.43207) = 0.38574$  for  $U_\kappa = 10^{-2}$  and  $U_\eta = 10^{-3}$ , as well as  $\sigma(z_{0,\max} = 0.44775) = 0.46054$  and  $\sigma_{T,\max}(z_{T,\max} = 0.42735) = 0.38711$  for  $U_\kappa = 10^{-8}$  and  $U_\eta = 10^{-12}$ . Since  $\sigma(z)$  has a greater maximum, the most unstable mode is localized in the vicinity of the point  $z_{0,\max}$  and according to the analytic results of Section 4 its wavenumber is established at  $k \sim U_\kappa^{-3/5}$ . The “dispersion relation”  $\sigma(k)$  for  $U_\kappa = 10^{-6}$  and  $U_\eta = 10^{-9}$  is shown on Figure 5, in which case the most unstable mode found from the numerical analysis has the growth

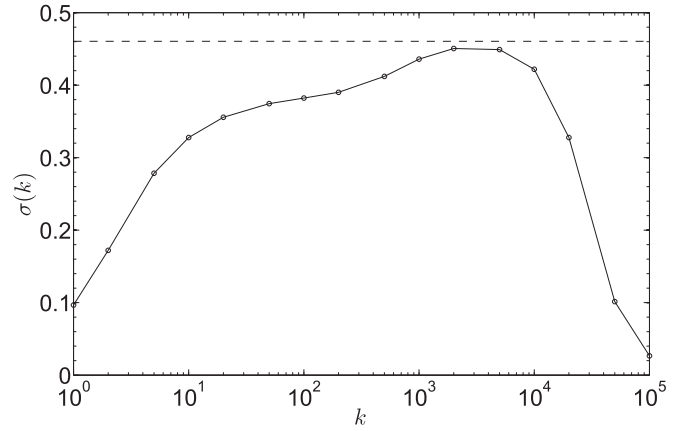


**Figure 5.** The relation between the numerically found growth rate  $\sigma$  and the wavenumber  $k$  for  $U_\kappa = 10^{-6}$ ,  $U_\eta = 10^{-9}$  and  $\Delta\bar{T} = 0.1$  (dots connected by a solid line); analytically found growth rate at the leading order,  $\sigma_0$  (dashed line). Other parameter values as on Figure 2.

rate  $\sigma_{\max} = 0.45292$  and the wavenumber  $k_{\max} = 3033 = 0.76 U_\kappa^{-3/5}$ . Let us examine more closely the actual distinguished balance in the Equation (80) that emerges in the numerical solution. The numerical values of all the terms in the braces multiplying  $w^{\text{BL}}(\xi)$  can be easily computed for all our numerical solutions. E.g., for  $U_\kappa = 10^{-8}$  and  $U_\eta = 10^{-12}$  we get  $\sigma_0(\sigma_0^2 - \sigma_T^2(z_{0,\max})) \approx 0.02782155$ ,  $\gamma F(\sigma_0^2 - \sigma_T^2(z_{0,\max}))k^2 U_\kappa / \bar{\rho} F_\gamma \approx -0.0566301$ ,  $\mathcal{P}\alpha\bar{T}\gamma(\sigma_0^2 - ((\gamma - 1)H_\rho^{-1} - H_\tau^{-1})/\gamma)k^2 U_\eta / F_\gamma \approx 5.1304 \times 10^{-4}$  and  $\sigma_0 \mathcal{P}\alpha\bar{T}\gamma k^4 U_\kappa U_\eta / \bar{\rho} F_\gamma \approx 0.02796597$ , which clearly indicates that the first and the last terms,  $0.02782155 + 0.02796597 = 0.05578752$  are in balance with the term  $\gamma F(\sigma_0^2 - \sigma_T^2(z_{0,\max}))k^2 U_\kappa / \bar{\rho} F_\gamma$  which determines the growth rate at the leading order. This observation is in very good agreement with the balance obtained for the partly asymptotic solution in Section 4. Note, that we have tried many runs to invalidate  $\sigma_0(\sigma_0^2 - \sigma_T^2(z_{0,\max})) \ll 1$  without success, thus the basic state solution seems to somehow possess this property.

The opposite regime corresponding to  $\sigma(z_{0,\max}) < \sigma_T(z_{T,\max})$  is presented on Figure 6 where the plots of the

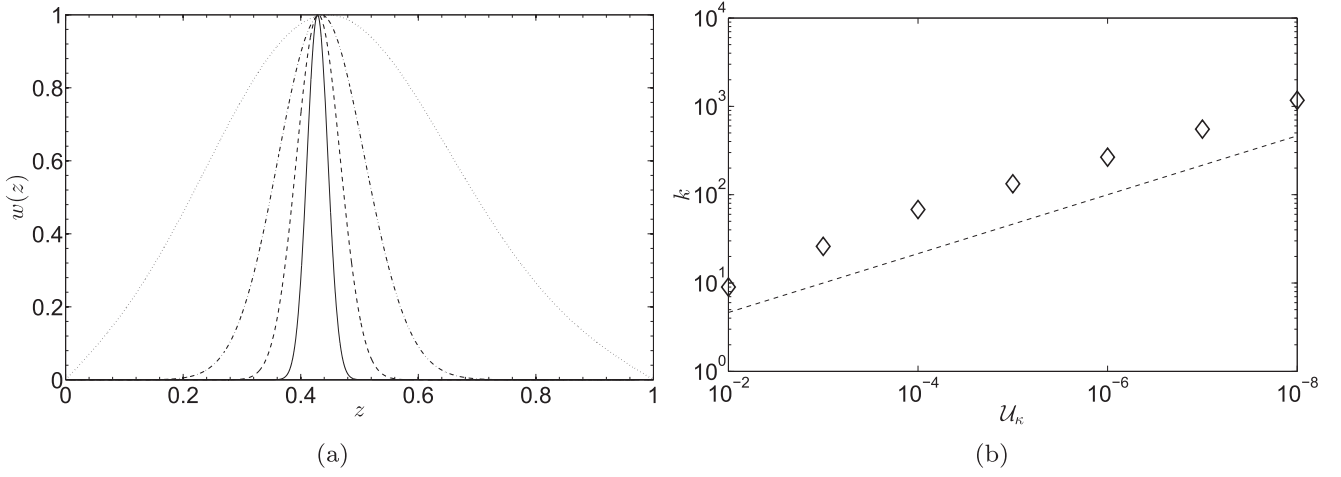


**Figure 6.** (a) Vertical velocity  $w(z)$  for the most unstable modes for  $\Delta\bar{T} = 0.2$  for:  $\mathcal{U}_\kappa = 10^{-2}$  and  $\mathcal{U}_\eta = 10^{-3}$  ( $k = 9$ ,  $\sigma = 0.37015$ ; solid line),  $\mathcal{U}_\kappa = 10^{-4}$  and  $\mathcal{U}_\eta = 10^{-6}$  ( $k = 68$ ,  $\sigma = 0.45669$ ; dashed line),  $\mathcal{U}_\kappa = 10^{-6}$  and  $\mathcal{U}_\eta = 10^{-9}$  ( $k = 266$ ,  $\sigma = 0.46916$ ; dotted-dashed line),  $\mathcal{U}_\kappa = 10^{-8}$  and  $\mathcal{U}_\eta = 10^{-12}$  ( $k = 1170$ ,  $\sigma = 0.47207$ ; dotted line). Other parameters values like at the Figure 2; (b) relation between the wavenumber  $k$  and thermal diffusivity  $\mathcal{U}_\kappa$ : numerical results (diamonds) and analytic relation  $k = \mathcal{U}_\kappa^{-1/3}$  (dashed line).  $\Delta\bar{T} = 0.2$ , other parameter values as on Figure 2.

vertical velocity  $w(z)$  and the  $k(\mathcal{U}_\kappa)$  dependence for the most unstable modes are provided for different values of the thermal and magnetic diffusivities and for  $\Delta\bar{T} = 0.2 > \Delta\bar{T}_{c1}$ . In that case the growth rate functions have the following maximum values:  $\sigma(z_{0,\max} = 0.43789) = 0.46067$  and  $\sigma_{T,\max}(z_{T,\max} = 0.43312) = 0.4717$  for  $\mathcal{U}_\kappa = 10^{-2}$  and  $\mathcal{U}_\eta = 10^{-3}$ , as well as  $\sigma(z_{0,\max} = 0.43696) = 0.46083$  and  $\sigma_{T,\max}(z_{T,\max} = 0.42822) = 0.47289$  for  $\mathcal{U}_\kappa = 10^{-8}$  and  $\mathcal{U}_\eta = 10^{-12}$ . Now it is the function  $\sigma_T(z)$  which has a greater maximum, and therefore the most unstable mode is localized in the vicinity of the point  $z_{T,\max}$  and its wavenumber is established at  $k \sim \mathcal{U}_\kappa^{-1/3}$ . The “dispersion relation”  $\sigma(k)$  for  $\mathcal{U}_\kappa = 10^{-6}$  and  $\mathcal{U}_\eta = 10^{-9}$  is shown on Figure 7 in which case the most unstable mode found from the numerical analysis has the growth rate  $\sigma_{\max} = 0.46916$  and the wavenumber  $k_{\max} = 266 = 2.66 \mathcal{U}_\kappa^{-1/3}$ .

The numerical results are in a good agreement with the theoretical predictions. It should also be emphasized, that the numerical analysis greatly helped to identify the interesting, partly asymptotic solution, which seems to naturally dominate when  $\sigma(z_{0,\max}) > \sigma_T(z_{T,\max})$ , since the maximal growth rates in this problem are typically smaller than unity, and the condition  $\sigma(z_{0,\max})(\sigma^2(z_{0,\max}) - \sigma_T^2(z_{0,\max})) \sim \mathcal{U}_\kappa^{1/10}$  (or  $\mathcal{U}_\kappa^{1/5}$  according to the footnote 2) required for the partly asymptotic solution to settle in is typically satisfied.

## 6. The 3D Case

In this section we present the leading-order analysis of the three-dimensional perturbations of the basic state described in Section 4, thus in the presence of magnetic and thermal diffusion related through (25). We will refer to the Section 6 in Mizerski et al. (2013), where the analysis of 3D modes for the isothermal and diffusionless system is presented. The main aims are to find the growth rate at the leading order, the criterion for instability with respect to 3D modes and a criterion for dominance of the 2D modes over the 3D ones.

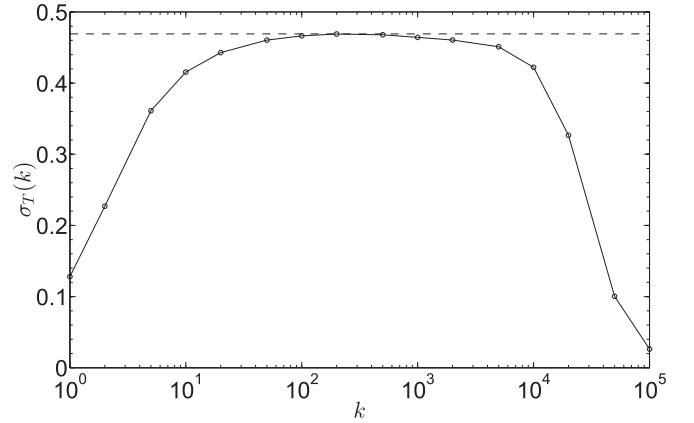


**Figure 7.** The relation between the numerically found growth rate  $\sigma$  and the wavenumber  $k$  for  $\mathcal{U}_\kappa = 10^{-6}$ ,  $\mathcal{U}_\eta = 10^{-9}$  and  $\Delta\bar{T} = 0.2$  (dots connected by a solid line); analytical found growth rate at the leading order,  $\sigma_0$  (dashed line). Other parameter values as on Figure 2.

We now introduce fully three-dimensional perturbations in the form

$$\begin{aligned} \mathbf{u} &= (u(z), v(z), w(z))e^{\sigma t + i(k_x x + k_y y)}, \\ \mathbf{b} &= (b_x(z), b_y(z), b_z(z))e^{\sigma t + i(k_x x + k_y y)}, \end{aligned} \quad (44a)$$

$$\begin{aligned} p &= \tilde{p}(z)e^{\sigma t + i(k_x x + k_y y)}, & \rho &= \tilde{\rho}(z)e^{\sigma t + i(k_x x + k_y y)}, \\ T &= \tilde{T}(z)e^{\sigma t + i(k_x x + k_y y)}. \end{aligned} \quad (44b)$$

into the Equations 1(a)–(f) and after linearization we obtain the following system of equations

$$\sigma \bar{p} u = -ik_x \mathcal{P} \tilde{p} + \Lambda \bar{B}' b_z, \quad (45a)$$

$$\sigma \bar{p} v = -ik_y (\mathcal{P} \tilde{p} + \Lambda \bar{B} b_x) + ik_x \Lambda \bar{B} b_y, \quad (45b)$$

$$\sigma \bar{p} w = -\tilde{\rho} - \frac{d}{dz} (\mathcal{P} \tilde{p} + \Lambda \bar{B} b_x) + ik_x \Lambda \bar{B} b_z, \quad (45c)$$

$$\sigma b_x = -ik_y \bar{B}v - \frac{d}{dz}(\bar{B}w) + \mathcal{U}_\eta \frac{d^2}{dz^2} b_x - \mathcal{U}_\eta (k_x^2 + k_y^2) b_x, \quad (45d)$$

$$\sigma b_y = ik_x \bar{B}v + \mathcal{U}_\eta \frac{d^2}{dz^2} b_y - \mathcal{U}_\eta (k_x^2 + k_y^2) b_y, \quad (45e)$$

$$\sigma b_z = ik_x \bar{B}w + \mathcal{U}_\eta \frac{d^2}{dz^2} b_z - \mathcal{U}_\eta (k_x^2 + k_y^2) b_z, \quad (45f)$$

$$\begin{aligned} \sigma \bar{\rho} \tilde{T} &= -\frac{(\gamma-1)\bar{p}}{\alpha} ik_x u - \frac{(\gamma-1)\bar{p}}{\alpha} ik_y v \\ &- \bar{\rho} \tilde{T}' w - \frac{(\gamma-1)\bar{p}}{\alpha} \frac{d}{dz} w \\ &+ \gamma \mathcal{U}_\kappa \frac{d^2}{dz^2} \tilde{T} - \gamma \mathcal{U}_\kappa (k_x^2 + k_y^2) \tilde{T} + \frac{2(\gamma-1)\Lambda \bar{B}'}{\mathcal{P}\alpha} \mathcal{U}_\eta \frac{d}{dz} b_x \\ &- \frac{2(\gamma-1)\Lambda \bar{B}'}{\mathcal{P}\alpha} \mathcal{U}_\eta ik_x \frac{d}{dz} b_z, \end{aligned} \quad (45g)$$

$$\sigma \bar{\rho} = -ik_x \bar{\rho} u - ik_y \bar{\rho} v - \frac{d}{dz}(\bar{\rho} w), \quad (45h)$$

$$\bar{\rho} = \alpha \bar{\rho} \tilde{T} + \alpha \tilde{T} \bar{\rho}, \quad (45i)$$

$$ik_x b_x + ik_y b_y + \frac{d}{dz} b_z = 0. \quad (45j)$$

It can be shown, that similarly as for the 2D modes (cf. Section 4), in the 3D case there are also two distinct main regimes, with different growth rates of the most unstable modes, which manifest depending on the magnitude of the temperature scale height. However, the value of the horizontal wavenumber  $k_x$  plays an important role. We consider only the two dynamical regimes corresponding to physically realistic settings as in 1i) and 2 in Section 4. Therefore the growth rate values of the 3D modes will be denoted by  $\sigma_{3D}$  and  $\sigma_{T3D}$  respectively and are defined below in (99) and (102). Details of the asymptotic analysis at large values of the horizontal wavenumber  $k_y \gg 1$  in the direction perpendicular to the applied field are described in Appendix D.

### 6.1. The Most Unstable 3D Mode for $\sigma_{3D} > \sigma_{T3D}$

In this regime the magnetic diffusion is negligible at the leading order and the thermal diffusion term in the energy equation dominates all others in the BL region, hence the system of governing equations becomes similar to the isothermal and diffusionless case described in Mizerski et al. (2013). The growth rate of the most unstable mode at the leading order takes the form (99). As stated, we study only the case of stably stratified fluid, that is  $H_\rho < 0$  and therefore we obtain the following criterion for instability of the 3D modes

$$k_x^2 < -\frac{\chi \bar{\rho}}{\Lambda \bar{B}^2} H_B^{-1} \equiv -\frac{1}{\mathcal{P}\alpha \bar{T}} H_B^{-1}, \quad (46)$$

where  $\chi = \Lambda \bar{B}^2 / (\mathcal{P}\alpha \bar{T} \bar{\rho})$  was defined in (32). The latter criterion exhibits similarity to the diffusionless, isothermal case (cf. Equation (71) in Mizerski et al. 2013). The long-wavelength modes in the  $x$ -direction are favored and they are

destabilized only by the magnetic field decreasing with height, just as in the isothermal case.

If the inequality (46) is satisfied and the system is unstable with respect to 3D modes, the same reasoning as in the Section 6.2 of Mizerski et al. (2013) leads to a conclusion, that the 2D (interchange) modes studied in Sections 4 and Appendix B.1 dominate over 3D modes if

$$\begin{aligned} -H_B^{-1} &> -(2 + \chi) H_\rho^{-1} \Leftrightarrow \\ -H_B^{-1} - \frac{(2 + \chi)}{(1 + \chi)^2} H_T^{-1} &> \frac{(2 + \chi)}{\mathcal{P}\alpha \bar{T} (1 + \chi)^2}, \end{aligned} \quad (47)$$

where in the latter formula the relation (33) was used. In stellar interiors, where  $\beta \gg 1$  and  $\alpha \sim 1$ , we have  $\chi \ll 1$  and we can simplify the criterion for domination of interchange modes to  $-H_B^{-1} \gtrsim -2H_\rho^{-1} \approx 0.8$  (cf. Gough 2007 for the value of  $H_\rho$  in the solar tachocline) in units of the tachocline thickness  $d \approx 3.5 \times 10^7$  m, or equivalently to  $-H_B^{-1} + 2/\mathcal{P}\alpha \bar{T} \gtrsim -H_B^{-1} - 2H_T^{-1} \gtrsim 2/\mathcal{P}\alpha \bar{T}$  according to (33) and our assumption  $H_\rho^{-1} < 0$ . Diffusionless and isothermal analog of the latter inequality, i.e.,  $-H_B^{-1} > (2 + \chi)/\mathcal{P}\alpha(1 + \chi)^2 \approx 2/\mathcal{P}\alpha$  (cf. Equation (73) in Mizerski et al. 2013) is more restrictive, therefore the presence of thermal effects relaxes the criterion for domination of the interchange modes. When  $\sigma_{3D} > \sigma_{T3D}$  and (47) are satisfied the most unstable mode is the partly asymptotic 2D interchange mode obtained in Sections 4 and 5 with  $\sigma_0 = \sigma(z_{0,\max})$  and  $k \sim \mathcal{U}_\kappa^{-3/5}$ .

### 6.2. The Most Unstable 3D Mode for $\sigma_{T3D} > \sigma_{3D}$

In this regime both the thermal and the magnetic diffusion are negligible at the leading order. The growth rate of the most unstable mode at the leading order takes the form (102). The criterion for instability with respect to 3D modes yields now

$$\begin{aligned} k_x^2 &< -\frac{\chi_\gamma \bar{\rho}}{\Lambda \bar{B}^2} (H_B^{-1} + \mathcal{H}^{-1}) \\ &\equiv -\frac{1}{\mathcal{P}\alpha \bar{T} \gamma} (H_B^{-1} + \mathcal{H}^{-1}), \end{aligned} \quad (48)$$

where

$$\begin{aligned} \mathcal{H}^{-1} &= \chi^{-1} (H_T^{-1} - (\gamma - 1) H_\rho^{-1}) \\ &= \chi^{-1} \left( \gamma H_T^{-1} + (\gamma - 1) \chi H_B^{-1} + \frac{\gamma - 1}{\mathcal{P}\alpha \bar{T}} \right), \end{aligned} \quad (49)$$

$\chi_\gamma = \Lambda \bar{B}^2 / (\mathcal{P}\alpha \bar{T} \gamma \bar{\rho})$  was defined in (31) and  $\mathcal{H}^{-1}$  is negative for a subadiabatic fluid layer. It is observed, that in this regime the 3D modes are destabilized not solely by  $H_B < 0$ , that is by the mean magnetic field decreasing with height, but the entire term  $\chi H_B^{-1} + H_T^{-1} - (\gamma - 1) H_\rho^{-1}$  must be negative, where  $H_\rho < 0$ . However, if the system is in a nearly adiabatic state, then  $H_T^{-1} - (\gamma - 1) H_\rho^{-1} \approx 0$  and the condition for destabilization of 3D modes reduces to  $H_B < 0$  and  $k_x^2 < -1/\mathcal{P}\alpha \bar{T} \gamma H_B$  which is similar, however less restrictive than (46). Nevertheless, it is of interest to provide also a general requirement for

the 3D instability to set in, which by (48) and (49) is

$$\frac{1}{\chi \mathcal{P} \alpha \bar{T}} > -H_B^{-1} - \chi^{-1} H_T^{-1} > \frac{\gamma - 1}{\gamma \chi \mathcal{P} \alpha \bar{T}} > 0, \quad (50)$$

where the left inequality results from (33) and our assumption  $H_\rho^{-1} < 0$ . As in the previous subsection we have a new criterion for domination of interchange modes

$$\begin{aligned} -(H_B^{-1} + \mathcal{H}^{-1}) &> -(2 + \chi_\gamma) H_\rho^{-1} \\ \Leftrightarrow -H_B^{-1} - \chi^{-1} H_T^{-1} &> \frac{2 + \chi_\gamma + (\gamma - 1) \chi^{-1}}{\gamma \mathcal{P} \alpha \bar{T} (1 + \chi_\gamma)^2}. \end{aligned} \quad (51)$$

In stellar interiors, for  $\chi \ll 1$  and  $\chi_\gamma \ll 1$ , we can simplify the criterion to  $-H_T^{-1} \gtrsim (\gamma - 1)/\gamma \mathcal{P} \alpha \bar{T}$ , which shows that in the current case it is the magnitude of the negative temperature gradient which mainly determines whether the 2D instability dominates. However, as remarked, in a nearly adiabatic layer  $\mathcal{H}^{-1} \approx 0$  and could be eliminated, which reduces the condition (51) to  $-H_B^{-1} > -(2 + \chi_\gamma) H_\rho^{-1}$  or equivalently  $-H_B^{-1} - (2 + \chi_\gamma) H_T^{-1} / (1 + \chi(2 + \chi_\gamma)) > (2 + \chi_\gamma) / \mathcal{P} \alpha \bar{T} (1 + \chi(2 + \chi_\gamma))$ . When  $\chi \ll 1$ ,  $\chi_\gamma \ll 1$  this gives  $-H_B^{-1} - 2H_T^{-1} \gtrsim 2/\mathcal{P} \alpha \bar{T}$  (i.e.,  $-H_B^{-1} \gtrsim 0.8$  for the solar tachocline), which is the same as the condition obtained in Section 6.1. When (51) is satisfied the most unstable mode is the 2D interchange mode obtained in Sections 4 and 5 characterized by  $\sigma_0 = \sigma_T(z_{T,\max})$ ,  $k \sim \mathcal{U}_\kappa^{-1/3}$ .

### 6.3. The Most Unstable Mode: Summary

Taking into account all the results of Sections 4–6, we are now ready to provide a general recipe to find the most unstable mode from among all the 2D (interchange) and 3D modes. In the limit of weak thermal and magnetic diffusivities we have found a criterion for the dominant type of 2D mode (cf. (83)) and for the domination of 2D instabilities over the 3D ones (cf. (47) and (51)).<sup>1</sup>

To find the most unstable mode, at first one needs to estimate the term  $\sigma(z_{0,\max})(\sigma^2(z_{0,\max}) - \sigma_T^2(z_{0,\max}))$ , where growth-rate functions are given in (39) and (40) to see, whether it is of the order  $\mathcal{U}_\kappa^{1/10}$  (or  $\mathcal{U}_\kappa^{1/5}$ ). If this is satisfied, then the next step is to find the maximum value among all the four growth-rate functions:  $\sigma(z)$  (39),  $\sigma_T(z)$  (40) and those obtained from the formulae (99) and (102), that is  $\sigma_{3D}(z)$  and  $\sigma_{T3D}(z)$ . This value, say  $\sigma_{\max}$ , is the growth rate of the most unstable mode and in case  $\sigma(z_{0,\max})$  dominates the most unstable mode is characterized by  $\sigma_{\max} = \sigma(z_{0,\max})$  and  $k \sim \mathcal{U}_\kappa^{-3/5}$  (and localized near  $z_{0,\max}$ ), whereas if  $\sigma_T(z_{T,\max})$  dominates we get  $\sigma_{\max} = \sigma_T(z_{T,\max})$  and  $k \sim \mathcal{U}_\kappa^{-1/3}$  (localization near  $z_{T,\max}$ ) for the most unstable mode. Alternatively it is enough to check the criteria (47) when  $\sigma_{3D} > \sigma_{T3D}$  and (51) for  $\sigma_{T3D} > \sigma_{3D}$  to determine at first, whether the 2D or the 3D modes dominate and in the former case determine the final dominant mode through the criterion (83). Figure 8 shows the growth rate functions  $\sigma(z)$ ,  $\sigma_T(z)$ ,  $\sigma_{3D}(z)$  and  $\sigma_{T3D}(z)$  for the set of parameter values chosen for numerical investigations of Section 5:  $\Delta \bar{T} = 0.2$ ,  $\alpha = 1.00$ ,  $\Lambda = 0.20$ ,  $\Delta \bar{B} = 1.35$ ,  $\mathcal{P} = 1.90$ , and  $\bar{\rho}(z=0) = 1.39$ , as well as diffusivities  $\mathcal{U}_\kappa = 10^{-8}$ ,  $\mathcal{U}_\eta = 10^{-12}$ . For the 3D functions on that plot, the horizontal

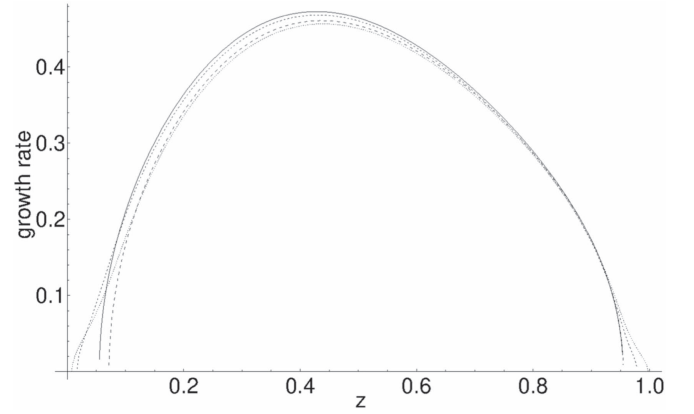


**Figure 8.** The growth-rate functions:  $\sigma(z)$  (thick-dashed line),  $\sigma_T(z)$  (solid line),  $\sigma_{3D}(z)$  (dotted line), and  $\sigma_{T3D}(z)$  (thin-dashed line) for  $\mathcal{U}_\kappa = 10^{-8}$ ,  $\mathcal{U}_\eta = 10^{-12}$ ,  $\Delta \bar{T} = 0.2$ ,  $\alpha = 1.00$ ,  $\Lambda = 0.20$ ,  $\Delta \bar{B} = 1.35$ ,  $\mathcal{P} = 1.90$ ,  $\bar{\rho}(z=0) = 1.39$ , and (for 3D case)  $k_x = 0.1$ .

wavenumber was set at  $k_x = 0.1$ . It can be seen that the functions are very similar. For the given set of parameters, the function  $\sigma_T(z)$  has the highest maximum value among all, and thus the most unstable mode will be the one with the growth rate  $\sigma_T(z_{T,\max})$  at the leading order. When  $k_x \rightarrow 0$ , we have  $\sigma_{3D}(z) \rightarrow \sigma(z)$  and  $\sigma_{T3D}(z) \rightarrow \sigma_T(z)$ , whereas according to criteria (46) and (48) for emergence of the 3D instability, the 3D instability is suppressed when  $k_x$  becomes too large.

In the case when the term  $\sigma(z_{0,\max})(\sigma^2(z_{0,\max}) - \sigma_T^2(z_{0,\max}))$  is of order unity, not  $\mathcal{U}_\kappa^{1/10}$  or  $\mathcal{U}_\kappa^{1/5}$  (a case we were unable to achieve numerically for reasons that are not fully understood) in the 2D case, only fully asymptotic solutions correspond to the most unstable mode. In such a case,  $\sigma_T(z_{T,\max})$  can again dominate, leading to  $\sigma_{\max} = \sigma_T(z_{T,\max})$  and  $k \sim \mathcal{U}_\kappa^{-1/3}$  for the most unstable mode, which is then 2D. On the other hand, if  $\sigma_{4/3}(z_{\max})$  happens to dominate, the most unstable mode is also 2D and is characterized by  $\sigma_{\max} = \sigma_{4/3}(z_{\max})$  and  $k \sim \mathcal{U}_\kappa^{-3/4}$ .

Finally, let us stress that the importance of the 3D instabilities for lower vertical field gradients in the solar tachocline has been demonstrated in previous studies, such as Newcomb (1961), Gilman (1970), and Acheson (1979). The physical picture that we have in mind is as follows. The shear in the tachocline has a certain, large magnitude, as is known from observations. This magnitude is determined regardless of any instabilities in the tachocline. This in turn produces a large vertical gradient of the magnetic field. Therefore, the magnitude of this gradient is mainly determined by the magnitude of shear,  $\mathbf{u}_P \cdot \nabla B_T \approx \mathbf{B}_P \cdot \nabla u_T \Rightarrow \partial_z B_T \approx (B_z/u_z) \partial_z u_T$ , where the subscripts  $T$  and  $P$  indicate the toroidal (azimuthal) and poloidal (vertical) components, respectively. Consequently, once the magnitude of the vertical gradient of the magnetic field is known, it can be determined whether its value is small enough for the 3D modes to dominate. We have shown above that the critical value of the vertical field gradient for transition between the 2D and 3D instabilities in the tachocline context is  $-H_B^{-1} \approx 0.8$ , and the 2D interchange modes dominate when the gradients are stronger.

In summary, the 2D modes are important in the dynamics as long as the shear, determined otherwise, possesses a large enough magnitude. Unfortunately, our linear analysis does not allow us to draw any definite conclusions about saturation, which is rather expected to become a 3D process at some point.

<sup>1</sup> A criterion for the dominant type among the 3D modes also exists and, in principle, could be derived, however, its form is very cumbersome.

Nevertheless, the presented analysis simply allows to understand how the fully 3D turbulence develops from initially growing 2D perturbations. Moreover, it is possible that a weakly nonlinear regime, which would then be strongly linked to the discovered mode structure, could be sufficient to develop some understanding of important dynamical aspects of the tachocline. As is explained in Section 4, the 2D modes are indeed localized in the vertical direction, but their vertical thickness is  $\delta \sim k^{-1/2}$ . Thus, for the most unstable modes for which the wavelengths were estimated at  $\lambda \sim 10^2$  km or  $\lambda \sim 1$  km, their vertical thickness is  $\delta \sim 1000 - 100$  km, which is small in comparison with the tachocline thickness  $d = 3.5 \times 10^4$  km, but not so much as to become dynamically unimportant.

## 7. Discussion

We have revisited the problem of short-wavelength magnetic buoyancy instability in a plane layer of fluid, introduced by Gilman (1970) and Acheson (1979) and studied the effect of weak thermal diffusivity and electric resistivity, which turned out to be quite diversified. We have assumed perfectly conducting and impermeable boundaries, and followed the asymptotic approach of Mizerski et al. (2013) to determine the spatial and temporal timescales of variation of the most unstable modes via the Rayleigh–Schrödinger perturbation technique. The main profit of the analysis is the determination of the short wavelengths of the most unstable modes through introduction of weak diffusivities, because the diffusive decay dominates the growth at short enough wavelengths, a phenomenon that strengthens with increasing wavenumber (cf. Mizerski et al. 2013) in the absence of diffusion. The analysis is fully comprehensive for the most unstable mode in the asymptotic limit  $k \gg 1$ ,  $\mathcal{U}_\eta \ll 1$  and  $\mathcal{U}_\kappa \ll 1$ . There are no gaps in the parameter domain. We have separately considered all possible cases for which the asymptotic relations between all the terms in the Equations (17) and (80) are different, and found a definite answer as to which of all the possible modes is the most unstable one under certain conditions determined by the basic state. However, there is a large variety of regimes and scalings corresponding to growth rates and spatial scales of variation of the most unstable modes. These are summarized at the end of Section 4 and in Section 6.3. A curious result is that, although the resistivity was always assumed much weaker than the thermal diffusivity (both related through  $\mathcal{U}_\eta \sim \mathcal{U}_\kappa^{3/2}$ ), the magnetic diffusion nevertheless plays a vital role in the dynamics. In particular, there exists a regime defined by  $\sigma(z_{0,\max}) > \sigma_T(z_{T,\max})$ ; when in the absence of magnetic diffusion, the wavelength of the most unstable mode can not be established. However, when weak resistivity is introduced, both diffusivities interact in an interesting way and the wavelength of the most unstable mode is determined at  $k \sim \mathcal{U}_\kappa^{-3/5}$  or  $k \sim \mathcal{U}_\kappa^{-3/4}$ , depending on the properties of the basic-state solution (cf. Section 4 and its summary at the end). The opposite regime,  $\sigma(z_{0,\max}) < \sigma_T(z_{T,\max})$ , has been shown, both analytically and numerically, to lead to  $k \sim \mathcal{U}_\kappa^{-1/3}$  for the most unstable mode.

Another interesting result is the identification of what we called a partly asymptotic solution, corresponding to the regime  $\sigma(z_{0,\max}) > \sigma_T(z_{T,\max})$ , shown analytically and numerically to dominate for diffusivities as low as  $\mathcal{U}_\kappa = 10^{-8}$  and  $\mathcal{U} = 10^{-12}$ , characterized by the growth rate of  $\sigma(z_{0,\max})$  and  $k \sim \mathcal{U}_\kappa^{-3/5}$ .

This solution requires  $\sigma(z_{0,\max})(\sigma^2(z_{0,\max}) - \sigma_T^2(z_{0,\max}))$  to be of either order  $\mathcal{U}_\kappa^{1/10}$  or  $\mathcal{U}_\kappa^{1/5}$ , which was satisfied in all our numerical simulations; interestingly, we were unable to find a different numerical solution, possibly due to the fact that the maximal growth rates found were always smaller than unity, and thus a term that involves the third power of such a number is necessarily quite small. A fully asymptotic solution in such a regime, which would replace the partly asymptotic one with diffusivities even smaller than  $\mathcal{U}_\kappa = 10^{-8}$  and  $\mathcal{U} = 10^{-12}$ , was also determined; it corresponds to the growth rate of  $\sigma_{4/3}(z_{\max})$  and  $k \sim \mathcal{U}_\kappa^{-3/4}$ .

The fully three-dimensional perturbations were also considered, and criteria for domination of the interchange modes were derived in Section 6. Similarly as in the isothermal and diffusionless case analyzed in Mizerski et al. (2013), the 3D modes are the dominant ones for weakly unstable magnetic field gradients, whereas the interchange modes take over at stronger field gradients. However, the influence of nonuniform temperature distribution is reported, and there exists a regime where the domination of the interchange or the 3D modes is mainly determined by the magnitude of the temperature gradient, with very little influence from the magnetic field gradient.

The magnetic buoyancy instabilities are often invoked in the context of stellar interiors, where the influence of velocity shear is crucial. That effect was not included in our investigations, but we plan to include it in future studies. In this sense, the presented analysis can be thought of as a step toward achieving a complete description of the full problem with shear and diffusivities, which could then reliably model the stellar interiors.

The authors wish to thank Professor David Hughes for fruitful discussions on this topic. Funding from the Ministry of Science and Higher Education of Poland within statutory activities No 3841/E-41/S/2015, grant no. IP 2014 031373 and funds from the Leading National Research Centre (KNOW) received by the Centre for Polar Studies in Poland for the period 2014–2018 are gratefully acknowledged.

## Appendix A

### Details of the 2D Asymptotic Analysis for $\mathcal{U}_\eta \ll 1$ , $\mathcal{U}_\kappa = \infty$

The coefficients  $\tilde{f}_i(z)$  of Equation (17) have the following form:

$$\tilde{f}_4(z) = \mathcal{U}_\eta k^{-2} \sigma f_{41}(z) + \mathcal{U}_\eta k^{-4} \sigma^3 f_{42}(z; \sigma^2), \quad (52a)$$

$$\tilde{f}_3(z) = \mathcal{U}_\eta k^{-2} \sigma f_{31}(z) + \mathcal{U}_\eta k^{-4} \sigma^3 f_{32}(z; \sigma^2), \quad (52b)$$

$$\begin{aligned} \tilde{f}_2(z) &= k^{-2} \sigma^2 f_{21}(z) + k^{-4} \sigma^4 f_{22}(z; \sigma^2) \\ &+ \mathcal{U}_\eta \sigma f_{23}(z) + \mathcal{U}_\eta k^{-2} \sigma^2 f_{24}(z; \sigma^2, \sigma^4) \\ &+ \mathcal{U}_\eta k^{-4} \sigma^3 f_{25}(z; \sigma^2, \sigma^4), \end{aligned} \quad (52c)$$

$$\begin{aligned} \tilde{f}_1(z) &= k^{-2} \sigma^2 f_{11}(z) + k^{-4} \sigma^4 f_{12}(z; \sigma^2) \\ &+ \mathcal{U}_\eta \sigma f_{13}(z) + \mathcal{U}_\eta k^{-2} \sigma^3 f_{14}(z; \sigma^2), \end{aligned} \quad (52d)$$

$$\begin{aligned} \tilde{f}_0(z) &= f_{01}(z; \sigma^2) + k^{-2} \sigma^2 f_{02}(z; \sigma^2, \sigma^4) \\ &+ k^{-4} \sigma^4 f_{03}(z; \sigma^2, \sigma^4) \\ &+ \mathcal{U}_\eta k^2 \sigma f_{04}(z) + \mathcal{U}_\eta \sigma f_{05}(z; \sigma^2, \sigma^4) \\ &+ \mathcal{U}_\eta k^{-2} \sigma^3 f_{06}(z; \sigma^2, \sigma^4), \end{aligned} \quad (52e)$$

where the functions  $\tilde{f}_{ij}(z)$  are dependent only on the basic-state functions, their derivatives, and the dimensionless parameters except  $\mathcal{U}_\eta$ . The functions  $\tilde{f}_{ij}(z; \sigma^\alpha)$  also include some terms proportional to  $\sigma^\alpha$ , where  $\alpha$  is a rational number.

It is clear that, in the considered limit  $k \gg 1$  and  $\mathcal{U}_\eta \ll 1$  at the leading order, the above functions can be approximated by the dominant terms only; the only functions that are utilized in Section 3 are:

$$f_4(z) = \left( \frac{\mathcal{P}\alpha}{F(z)} \right) \sigma k^{-2} \mathcal{U}_\eta, \quad (53a)$$

$$f_2(z) = -k^{-2} \sigma^2 - \left( \frac{2\mathcal{P}\alpha}{F(z)} \right) \sigma \mathcal{U}_\eta, \quad (53b)$$

$$f_0(z) = \left( \sigma^2 - \frac{\Lambda \bar{B}^2(z)}{F(z) \bar{\rho}(z)} (H_\rho^{-1}(z) - H_B^{-1}(z)) \right) + \left( \frac{\mathcal{P}\alpha}{F(z)} \right) \sigma k^2 \mathcal{U}_\eta. \quad (53c)$$

Equation (17) contains two asymptotically small parameters, namely the inverse wavenumber (the wavelength)  $k^{-1} \ll 1$  and the magnetic diffusivity  $\mathcal{U}_\eta \ll 1$ , which are assumed to be related through a simple scaling law

$$k \sim \mathcal{U}_\eta^{-1/n}, \quad (54)$$

for some  $n > 0$ , to be established. This assumption, later validated by the asymptotic approach (and numerical simulations), is simply a convenient way to mathematically relate two positive quantities, which are expected to be related in the considered asymptotic regime. Parameters  $n$  (and  $m$  in relations (56) and (81) below) are used only to conveniently describe the different cases corresponding to distinct balances of terms in the equations, because all possibilities need to be considered in order to prove the final results for most unstable modes.

The presence of small parameters ( $k^{-1}$  and  $\mathcal{U}_\eta$ ) in the  $z$ -dependent coefficients in (17) suggests that the solutions become localized in the vicinity of some specific point corresponding to maximal growth rate in the system and adopt a boundary/internal layer form, just as in the ideal case in Mizerski et al. (2013).

The main aim of the current analysis is to identify the most unstable mode (its form and growth rate  $\sigma$ ) and the scaling law for the horizontal variation length scale of perturbations given by the relation (54). Therefore, we investigate Equation (17) for all  $n > 0$ , utilizing the BL method in a way similar to how it was described in Mizerski et al. (2013).

Let us therefore quickly summarize the mathematical procedure. We consider separate cases corresponding to different intervals of  $n \in (0, \infty)$  for which asymptotic relations between terms in Equation (17) are different. In each case, we use the method of dominant balance to analyze the equation in the main flow region (MF), i.e., outside the BLs where the  $z$ -derivatives of  $b_x(z)$  are of order unity, and in the (possibly internal) BL that forms in the vicinity of a certain point  $z_{\max}$  within the flow  $0 \leq z_{\max} \leq 1$ , which is determined from the requirement of growth-rate maximization. In the MF, where the leading-order term of the magnetic field perturbation will be denoted by  $b_x^{\text{MF}}(z)$ , the dominant balance determines the growth rate as a function of  $z$ , which can then be maximized to determine  $z_{\max}$ . On the other hand, we define a

scaled variable in the BL

$$\xi = \frac{z - z_{\max}}{\delta}, \quad (55)$$

where  $\delta = \delta(\mathcal{U}_\eta)$  denotes the thickness of the BL, i.e., the length scale for vertical variation of the perturbations. Thus, for every  $n > 0$  there exists some  $m > 0$  that allows to define the thickness  $\delta$  in terms of the small parameters  $\mathcal{U}_\eta$  or  $k^{-1}$ ,

$$\delta \sim \mathcal{U}_\eta^{m/n} \sim k^{-m}. \quad (56)$$

In the boundary-internal layer, all basic-state functions are evaluated at  $z = z_{\max}$ , and the magnetic field perturbation  $b_x(\xi)$  and the growth rate  $\sigma$  are expanded in powers of  $\delta$ , i.e.,  $\sigma = \sigma_0 + \delta\sigma_1 + \delta^2\sigma_2 + \dots$ , where  $\sigma_j = \mathcal{O}(1)$  for all non-negative integers  $j$ . Just as for the MF region, we only take the leading-order term of the magnetic field perturbation, which we denote as  $b_x^{\text{BL}}(\xi)$ .

We require that the solutions are smooth, and because (17) is a fourth-order ordinary differential equation, the following matching conditions at the point  $z_{\max}$  (ergo locally at  $\xi = 0$ ) are imposed:

$$\left. \frac{d^j b_x^{\text{BL}}(\xi)}{d\xi^j} \right|_{\xi \rightarrow 0^-} = \left. \frac{d^j b_x^{\text{BL}}(\xi)}{d\xi^j} \right|_{\xi \rightarrow 0^+}, \quad (57)$$

$$\left. \frac{d^j b_x^{\text{MF}}(z)}{dz^j} \right|_{z \rightarrow z_0^-} = \left. \frac{d^j b_x^{\text{BL}}(\xi)}{d\xi^j} \right|_{\xi \rightarrow -\infty}, \quad (58a)$$

$$\left. \frac{d^j b_x^{\text{MF}}(z)}{dz^j} \right|_{z \rightarrow z_0^+} = \left. \frac{d^j b_x^{\text{BL}}(\xi)}{d\xi^j} \right|_{\xi \rightarrow +\infty}, \quad (58b)$$

for  $\delta \rightarrow 0^+$  and  $j = 0, \dots, 4$ , with  $j = 0$  corresponding to the functions themselves, i.e.,  $b_x^{\text{MF}}(z)$  or  $b_x^{\text{BL}}(\xi)$ . Finally, we find the only possible distinguished limit in each case and investigate whether it allows to determine the growth rate.

Three separate cases need to be analyzed:  $n < 2$ ,  $n = 2$ , and  $n > 2$ . As will be shown below, it is the last one that leads to the most unstable mode. In the other cases, either the perturbations grow at a slower rate or no distinguished balance is possible.

#### A.1. Case $n < 2$

In such a case, the wavenumber satisfies  $k \gg \mathcal{U}_\eta^{-1/2}$ . Thus, from Equation (17), the term without the derivative of  $b_x(z)$  dominates in the MF. The equation reduces to

$$[\mathcal{U}_\eta k^2 \sigma f_{04}(z)] b_x^{\text{MF}}(z) = 0, \quad (59)$$

which means that either  $\sigma = 0$  or  $b_x^{\text{MF}}(z) = 0$  in the MF.

Inside the BL, Equation (17) reduces to

$$[k^{-4} \delta^{-4}] \frac{d^4}{d\xi^4} b_x^{\text{BL}}(\xi) - [2k^{-2} \delta^{-2}] \frac{d^2}{d\xi^2} b_x^{\text{BL}}(\xi) + b_x^{\text{BL}}(\xi) = 0. \quad (60)$$

Here, we get two cases: either one of the terms dominates all others, or the only possible balance between at least two terms is obtained for  $m = 1$  i.e.,  $\delta \sim k^{-1}$  and it contains all three terms. The former case does not lead to solutions that could be matched with  $b_x^{\text{MF}}(z) = 0$  in the limit  $\xi \rightarrow \pm\infty$ . For the latter case, the only solution possible to match (localized around

some  $0 < z_0 < 1$ ) is

$$b_x^{\text{BL}}(\xi) = \begin{cases} A(1 - \xi)e^{(k\delta)\xi} & \xi < 0 \\ A(1 + \xi)e^{-(k\delta)\xi} & \xi \geq 0, \end{cases} \quad (61)$$

where  $A$  is a constant that remains undetermined. The matching conditions for the first and second derivative of  $b_x^{\text{BL}}(\xi)$  were used. However, there is no  $\sigma_0$  in Equation (60) and the solution has a discontinuous third derivative. Hence, there are no smooth solutions in this case.

#### A.2. Case $n = 2$

When  $n = 2$ , the wavenumber satisfies  $k \sim \mathcal{U}_\eta^{-1/2}$ . Thus, from Equation (17), the term without the derivative still dominates in the MF region. The equation reduces to

$$\left[ \sigma^2 - \sigma^2(z) + \mathcal{U}_\eta k^2 \sigma \frac{\mathcal{P}\alpha}{F(z)} \right] b_x^{\text{MF}}(z) = 0. \quad (62)$$

Therefore, the only way to satisfy Equation (62) is for  $b_x^{\text{MF}}(z)$  to be zero.

Inside the BL, Equation (17) takes the following form

$$\begin{aligned} & \left[ \mathcal{U}_\eta k^{-2} \delta^{-4} \sigma_0 \frac{\mathcal{P}\alpha}{F(z_0)} \right] \frac{d^4}{d\xi^4} b_x^{\text{BL}}(\xi) \\ & - \left[ k^{-2} \delta^{-2} \sigma_0^2 + \mathcal{U}_\eta \delta^{-2} \sigma_0 \frac{2\mathcal{P}\alpha}{F(z_0)} \right] \frac{d^2}{d\xi^2} b_x^{\text{BL}}(\xi) \\ & + \left[ \sigma_0^2 - \sigma^2(z_0) + \mathcal{U}_\eta k^2 \sigma_0 \frac{\mathcal{P}\alpha}{F(z_0)} \right] b_x^{\text{BL}}(\xi) = 0, \end{aligned} \quad (63)$$

where  $z_0$  is the point where  $\sigma = \sqrt{\sigma^2(z_0) + (k^2 \mathcal{U}_\eta \mathcal{P}\alpha / 2F(z_0))^2} - k^2 \mathcal{U}_\eta \mathcal{P}\alpha / 2F(z_0)$  for the mode associated with a specific eigenvalue  $\sigma$ .

Three distinct ranges of parameter  $m$ , defined in (56), lead to different types of balance in the Equation (63):

1.  $m > 1$ : the first term dominates, and therefore the equation simplifies to  $\frac{d^4 b_x^{\text{BL}}(\xi)}{d\xi^4} = 0$ , which does not provide solutions that could be asymptotically matched with the zero MF solution.
2.  $m < 1$ : the third term dominates, hence we get the equation  $\left[ \sigma_0^2 - \sigma^2(z_0) + \mathcal{U}_\eta k^2 \sigma_0 \frac{\mathcal{P}\alpha}{F(z_0)} \right] b_x^{\text{BL}}(\xi) = 0$ , which determines the leading-order term of the growth rate as

$$\sigma_0 = \sqrt{\sigma^2(z_0) + \left( \mathcal{U}_\eta k^2 \frac{\mathcal{P}\alpha}{2F(z_0)} \right)^2} - \mathcal{U}_\eta k^2 \frac{\mathcal{P}\alpha}{2F(z_0)}. \quad (64)$$

This expression is always smaller than  $\sigma(z_0)$ ; hence the solution, if it exists, does not correspond to the most unstable mode.

3.  $m = 1$ : this is the only possible balance between at least two terms in (63) and it contains all three terms from this equation. Therefore, we need to consider Equation (63) in full, and we get several cases. First, we can assume a constant solution, which means that the coefficient  $\left[ \sigma_0^2 - \sigma^2(z_0) + \mathcal{U}_\eta k^2 \sigma_0 \frac{\mathcal{P}\alpha}{F(z_0)} \right]$  has to vanish. This case is the same as the one above for  $m < 1$ . Second, we can assume that the coefficient next to  $b_x^{\text{BL}}(\xi)$  has to be zero, which leads to non-trivial solutions in the following form

(for some constant  $\alpha, A_i, B_i$ )

$$b_x^{\text{BL}}(\xi) = \begin{cases} A_1 e^{\alpha\xi} + A_2 \xi + A_3 & \xi < 0, \\ B_1 e^{-\alpha\xi} + B_2 \xi + B_3 & \xi \geq 0. \end{cases} \quad (65)$$

However, this function can be of class  $C^0([0, 1])$  at most, and thus there are no smooth solutions of such type. Third, we can assume that the coefficient next to the second derivative vanishes,  $\left[ k^{-2} \delta^{-2} \sigma_0^2 + \mathcal{U}_\eta \delta^{-2} \sigma_0 \frac{2\mathcal{P}\alpha}{F(z_0)} \right] = 0$ , and solve (63); however, this leads to  $\sigma_0 < 0$ . Lastly, we can solve the full Equation (63) with non-zero coefficients, which leads to a solution in the form

$$b_x^{\text{BL}}(\xi) = \begin{cases} C \left( \frac{\alpha_1}{\alpha_2} e^{\alpha_2 \xi} - e^{\alpha_1 \xi} \right) & \xi < 0 \\ C \left( \frac{\alpha_1}{\alpha_2} e^{-\alpha_2 \xi} - e^{-\alpha_1 \xi} \right) & \xi \geq 0 \end{cases} \quad (66)$$

for some non-zero constants  $C, \alpha_1, \alpha_2$ . This solution has a discontinuous third derivative and does not lead to any condition for  $\sigma_0 > 0$ .

In conclusion, when  $n = 2$ , a positive growth rate is possible only for the case of  $m \leq 1$  and constant  $b_x^{\text{BL}}(\xi)$ , which leads to  $\sigma_0 < \sigma(z_0)$ . Because the results of Section 3 show that there exist modes with the growth rate  $\sigma(z_0)$ , the case  $n = 2$  does not lead to the most unstable mode.

#### A.3. Case $n > 2$

We will now demonstrate, that the most unstable mode appears when  $n > 2$ , and thus within a range of wavenumbers bounded from above,  $k \ll \mathcal{U}_\eta^{-1/2}$ . In such a regime, the term without derivatives of  $b_x^{\text{MF}}(z)$  in the MF Equation (17) dominates and the equation reduces to

$$[\sigma^2 - \sigma^2(z)] b_x^{\text{MF}}(z) = 0, \quad (67)$$

which can be understood as a depth-dependent dispersion relation (see Mizerski et al. 2013). The function  $\sigma(z)$  is the so-called ‘‘growth-rate function’’ defined in (18). Because the MF Equation (67) has the form of a vanishing product of a function of  $z$  multiplying the magnetic field  $b_x^{\text{MF}}(z)$ , the only way to satisfy Equation (67) is for  $b_x^{\text{MF}}(z)$  to be zero everywhere in the MF. Thus, the situation is reminiscent of the non-diffusive case, i.e., the most unstable eigenmode localizes in the vicinity of  $z_{\text{max}}$ , where a boundary/internal layer is formed, because the relation  $\sigma \approx \sigma(z_{\text{max}})$  can be approximately satisfied and hence the magnetic field in (67) can be non-trivial in this region.

For  $n > 2$  inside the BL, Equation (17) expressed in terms of the scaled variable  $\xi$  (55), reduces to

$$\begin{aligned} & \left[ \mathcal{U}_\eta k^{-2} \delta^{-4} \sigma_0 \frac{\mathcal{P}\alpha}{F(z_{\text{max}})} \right] \frac{d^4}{d\xi^4} b_x^{\text{BL}}(\xi) \\ & - [k^{-2} \delta^{-2} \sigma_0^2] \frac{d^2}{d\xi^2} b_x^{\text{BL}}(\xi) \\ & + \left[ \sigma_0^2 - \sigma^2(z_{\text{max}}) + \mathcal{U}_\eta k^2 \sigma_0 \frac{\mathcal{P}\alpha}{F(z_{\text{max}})} \right] b_x^{\text{BL}}(\xi) = 0, \end{aligned} \quad (68)$$

for the most unstable mode associated with the eigenvalue  $\sigma \approx \sigma(z_{\text{max}})$ , and  $\sigma_0$  is the leading-order term in the growth-rate



expansion in powers of the BL thickness  $\delta$ . We note here that Equation (17) can, in fact, also be satisfied by oscillatory modes with large  $z$ -derivatives in a significant part of the domain. However, such modes, examined in the Appendix of Mizerski et al. (2013) with the use of the WKB method, require at least one turning point, i.e.,  $\sigma$  must be less than  $\sigma(z)$  in a finite domain. Therefore, these modes are never the most unstable ones. Furthermore, numerical simulations of Mizerski et al. (2013) have clearly shown that evolution of the analyzed linear system from some initial state, even localized far from the point of maximum value of the growth rate function, becomes quite quickly dominated by the most unstable mode localized in the vicinity of  $z_{\max}$ . Thus, here we concentrate only on the most unstable modes.

Because the BL thickness  $\delta$ , related to the wavenumber  $k$  and magnetic diffusivity through the relation (56), is yet unknown, we have to consider all possible forms of balance between terms in Equation (68). There are three cases: two of them, namely  $m = 1/2 + n/4$  and  $m = n/2$ , do not lead to smooth solutions (which can be easily shown in way analogous to Appendices A.1 and A.2). The last one, with  $m = 1$ , i.e.,  $\delta \sim k^{-1}$ , corresponds to balance between the second and third terms in (68). For that case, the BL Equation (68) has the following form

$$[k^{-2}\delta^{-2}\sigma_0^2] \frac{d^2}{d\xi^2} b_x^{\text{BL}}(\xi) + [\sigma_0^2 - \sigma^2(z_{\max})] b_x^{\text{BL}}(\xi) = 0, \quad (69)$$

which is analogous to Equation 33(a) in Mizerski et al. (2013). Therefore, as in Mizerski et al. (2013), the only possible sufficiently smooth solution (which can be later matched with the zero solution in MF through internal layers) is a constant function denoted by  $b_x^{\text{BL}}(\xi) = B_x^{\text{BL}}$  with the leading-order term of the growth rate  $\sigma_0$  for the most unstable mode localized in a vicinity of  $z_{\max}$  given by  $\sigma_0^2 = \sigma^2(z_{\max})$ , which turns out to be the same formula as in the non-diffusive case (cf. (35) in Mizerski et al. 2013). Thus, another boundary/internal layer must be introduced to match this constant solution  $B_x^{\text{BL}}$  with  $b_x^{\text{MF}}(z) = 0$  in the MF.

However, before proceeding any further, we briefly summarize the final results of the analysis at the leading order. When  $n > 2$  and  $m = 1$ , i.e.,  $\delta \sim k^{-1} \sim \mathcal{U}_\eta^{1/n} \gg \mathcal{U}_\eta^{1/2}$ , the growth rate at the leading order is  $\sigma_0 = \sigma(z_{\max}) > 0$  and it is the greatest real positive one among any  $n > 0$ ,  $m > 0$ . Therefore, this growth rate is associated with the most unstable mode, which is localized in the vicinity of the point  $z_{\max}$  at which the growth-rate function takes its maximum value  $\sigma(z_{\max})$ .

Returning to the analysis, we will now assume that the function  $\sigma(z)$  (defined by (18)) has a quadratic maximum at  $z = z_{\max}$  with  $0 < z_{\max} < 1$ , and hence  $\frac{d}{dz}\sigma^2(z) \Big|_{z=z_{\max}} = 0$  and

$\frac{d^2}{dz^2}\sigma^2(z) \Big|_{z=z_{\max}} < 0$ . The most unstable mode is the one associated with the highest growth rate given by (19). It can be shown that, under these assumptions (supplied by the matching conditions (57) and (58)), one obtains the most unstable mode for  $\sigma_1 = 0$ , thus  $\sigma = \sigma_0 + \delta^2\sigma_2 + o(\delta^2)$ . This yields the

internal layer Equation (68) in the following form

$$\begin{aligned} & \left[ \mathcal{U}_\eta k^{-2} \delta^{-4} \sigma_0 \frac{\mathcal{P}\alpha}{F(z_{\max})} \right] \frac{d^4}{d\xi^4} b_x^{\text{BL}}(\xi) \\ & - [k^{-2} \delta^{-2} \sigma_0^2] \frac{d^2}{d\xi^2} b_x^{\text{BL}}(\xi) \\ & + \left[ 2\delta^2 \sigma_0 \sigma_2 + \mathcal{U}_\eta k^2 \sigma_0 \frac{\mathcal{P}\alpha}{F(z_{\max})} \right. \\ & \left. - \frac{1}{2} \delta^2 \xi^2 \frac{d^2}{dz^2} \sigma^2(z) \Big|_{z=z_{\max}} \right] b_x^{\text{BL}}(\xi) = 0, \quad (70) \end{aligned}$$

where the  $z$ -dependent functions have been expanded in Taylor series around  $z = z_{\max}$ . The Equation (70) is analogous to the Equation 33(c) in Mizerski et al. (2013); however, the former also contains a fourth-order derivative of the magnetic field perturbation and a new constant term  $\mathcal{U}_\eta k^2 \sigma_0 \mathcal{P}\alpha / F(z_{\max})$  in the coefficient at the term without the derivative. Because we are looking for the structure of the most unstable mode, Equation (70) is investigated for all distinguished limits for  $n > 2$  and  $m > 0$ . The only limits that lead to smooth eigenmodes without being self-contradictory are obtained for  $n \geq 3$  and  $m = 1/2$ .

For  $n > 3$  and  $m = 1/2$ , one obtains  $k \sim \mathcal{U}_\eta^{-1/n} \ll \mathcal{U}_\eta^{-1/3}$ , and  $\delta \sim \mathcal{U}_\eta^{1/2n} \gg \mathcal{U}_\eta^{1/6}$ ; Equation (70) takes the following form

$$\begin{aligned} & [k^{-2} \delta^{-2} \sigma_0^2] \frac{d^2}{d\xi^2} b_x^{\text{BL}}(\xi) \\ & - \left[ 2\delta^2 \sigma_0 \sigma_2 - \frac{1}{2} \delta^2 \xi^2 \frac{d^2}{dz^2} \sigma^2(z) \Big|_{z=z_0} \right] b_x^{\text{BL}}(\xi) = 0. \quad (71) \end{aligned}$$

The solution of the latter equation was presented in Section 4.1 of Mizerski et al. (2013). We get the same result as (38) in that paper, which is

$$\sigma_2 = -\frac{1}{2\sqrt{2}} k^{-1} \delta^{-2} \sqrt{-\frac{d^2}{dz^2} \sigma^2(z) \Big|_{z=z_0}}. \quad (72)$$

Therefore,  $\sigma_2 < 0$ , and of course  $|\sigma_2| \sim 1$  by assumption.

On the other hand, for  $n = 3$  and  $m = 1/2$ , the exponents in relations (54) and (56) can be easily determined to yield  $k^{-1} \sim \mathcal{U}_\eta^{1/3}$  and  $\delta \sim \mathcal{U}_\eta^{1/6}$ . In this regime, Equation (70) simplifies to

$$\begin{aligned} & [k^{-2} \delta^{-2} \sigma_0^2] \frac{d^2}{d\xi^2} b_x^{\text{BL}}(\xi) - \left[ 2\delta^2 \sigma_0 \sigma_2 + \mathcal{U}_\eta k^2 \sigma_0 \frac{\mathcal{P}\alpha}{F(z_{\max})} \right. \\ & \left. - \frac{1}{2} \delta^2 \xi^2 \frac{d^2}{dz^2} \sigma^2(z) \Big|_{z=z_{\max}} \right] b_x^{\text{BL}}(\xi) = 0, \quad (73) \end{aligned}$$

which leads to

$$\begin{aligned} \sigma_2 = & -\frac{1}{2\sqrt{2}} k^{-1} \delta^{-2} \sqrt{-\frac{d^2}{dz^2} \sigma^2(z) \Big|_{z=z_{\max}}} \\ & - \mathcal{U}_\eta k^2 \delta^{-2} \frac{\mathcal{P}\alpha}{2F(z_{\max})}, \quad (74) \end{aligned}$$

and the leading-order form of the magnetic field perturbation expressed in terms of the global variable  $z$  takes the form

$$b_{x,0}(z) = b_x^{\text{MF}}(z) + b_x^{\text{BL}}(z = \xi\delta + z_0) \\ = C \exp\left(-\frac{(z - z_{\text{max}})^2}{2\sqrt{2}}k\sigma_0^{-1/2}\left(-\frac{d^2}{dz^2}\sigma^2(z)\Big|_{z=z_{\text{max}}}\right)^{1/4}\right), \quad (75)$$

where  $C$  is an undetermined constant and  $b_x^{\text{BL}}(\xi \rightarrow \pm\infty) = b_x^{\text{MF}}(z) = 0$  (for details of the method of matching asymptotic expansions, see chapter 9 in Bender & Orszag 1978).

Comparison of Equations (72) and (74), i.e., the order  $\delta^2$  corrections to the growth rate for  $n > 3$  and  $n = 3$ , leads to a conclusion that, in both cases, the correction  $\sigma_2$  in the expansion  $\sigma = \sigma_0 + \delta^2\sigma_2 + o(\delta^2)$  is negative, but the BL thickness  $\delta$  is different in each of the cases. In the case  $n = 3$ , the BL thickness is asymptotically smaller than for  $n > 3$  because  $\delta_{n=3} = \mathcal{U}_\eta^{1/6} \ll \delta_{n>3} = \mathcal{U}_\eta^{1/2n}$ . Therefore, it can be concluded that the growth rate of the mode obtained for  $n = 3$  is asymptotically greater, than that obtained for any finite  $n > 3$  (the negative correction proportional to  $\mathcal{U}_\eta k^2 \delta^{-2}$  in (74) does not appear in formula (72) because for  $n > 3$  it is of the order  $\mathcal{U}_\eta^{1-3/n} \ll 1$ , and only at  $n = 3$  does it reach the order of unity). Hence, it is the case of  $n = 3$  that leads to the most unstable mode with  $k \sim \mathcal{U}_\eta^{-1/3}$ .

The formulae (72) and (74) for  $\sigma_2$  were obtained as part of solution of Equations (71) and (73), which can be transformed into the parabolic cylinder equation (see Abramowitz & Stegun 1972)

$$\frac{d^2}{dx^2}b_x^{\text{BL}}(x) - \left[\frac{1}{4}x^2 + a\right]b_x^{\text{BL}}(x) = 0, \quad (76)$$

where

$$x = \xi \left( \frac{2k^2\delta^4}{\sigma_0} \sqrt{-\frac{d^2}{dz^2}\sigma^2(z)\Big|_{z=z_0}} \right)^{1/4}, \quad (77)$$

and

$$a = \sqrt{2}k\delta^2\sigma_2 \left( -\frac{d^2}{dz^2}\sigma^2(z)\Big|_{z=z_0} \right)^{-1/2}, \quad (78)$$

for Equation (71) or

$$a = \sqrt{2}k\delta^2\sigma_2 \left( -\frac{d^2}{dz^2}\sigma^2(z)\Big|_{z=z_0} \right)^{-1/2} \\ + \mathcal{U}_\eta k^3 \frac{\sqrt{2}\mathcal{P}\alpha}{2F(z_0)} \left( -\frac{d^2}{dz^2}\sigma^2(z)\Big|_{z=z_0} \right)^{-1/2}, \quad (79)$$

for Equation (73). For the most unstable mode, one needs the smallest possible  $|\sigma_2|$  ( $\sigma_2 < 0$ ), which is obtained by taking the largest possible  $a$ , namely  $a = -1/2$  (see details in Section 3 of Mizerski et al. 2013). This establishes the value of  $\sigma_2$  given by in (72) and (74).

## Appendix B

### Details of the 2D Asymptotic Analysis for $\mathcal{U}_\eta \sim \mathcal{U}_\kappa^{3/2} \ll 1$

Application of scalings (37) and (38) to the set of perturbation Equations 35(a)–(f) in the asymptotic limit  $\mathcal{U}_\eta \sim \mathcal{U}_\kappa^{3/2} \ll 1$  allows to transform the equations into one second-order ordinary differential equation for the leading-order term of the vertical velocity perturbation in the BL around a given point  $z_0$  with  $\xi = (z - z_0)/\delta$ ; namely, for  $w^{\text{BL}}(\xi)$ ,

$$0 = \left[ \sigma^3 \delta^{-2} k^{-2} + \frac{\gamma F}{\bar{\rho} F_\gamma} \left( 2\sigma^2 - \frac{\Lambda \bar{B}^2}{\bar{\rho} F} (H_\rho^{-1} - H_B^{-1}) \right) \right] \delta^{-2} \mathcal{U}_\kappa \\ + \frac{\mathcal{P}\alpha \bar{T}\gamma}{F_\gamma} \left( 2\sigma^2 - \frac{\gamma - 1}{\gamma} \left( H_\rho^{-1} - \frac{H_T^{-1}}{\gamma - 1} \right) \right) \delta^{-2} \mathcal{U}_\eta \\ + \left( \frac{3\sigma \mathcal{P}\alpha \bar{T}\gamma}{\bar{\rho} F_\gamma} \right) \delta^{-2} k^2 \mathcal{U}_\eta \mathcal{U}_\kappa \left] \frac{d^2}{d\xi^2} w^{\text{BL}}(\xi) \\ - \left[ \sigma^3 - \frac{\sigma \Lambda \bar{B}^2}{\bar{\rho} F_\gamma} (H_\rho^{-1} - H_B^{-1}) \right. \\ \left. - \frac{\sigma \mathcal{P}\alpha \bar{T}(\gamma - 1)}{F_\gamma} \left( H_\rho^{-1} - \frac{H_T^{-1}}{\gamma - 1} \right) \right. \\ \left. + \left( \frac{\sigma^2 \gamma F}{\bar{\rho} F_\gamma} - \frac{\gamma \Lambda \bar{B}^2}{\bar{\rho}^2 F_\gamma} (H_\rho^{-1} - H_B^{-1}) \right) k^2 \mathcal{U}_\kappa \right. \\ \left. + \frac{\mathcal{P}\alpha \bar{T}\gamma}{F_\gamma} \left( \sigma^2 - \frac{\gamma - 1}{\gamma} \left( H_\rho^{-1} - \frac{H_T^{-1}}{\gamma - 1} \right) \right) k^2 \mathcal{U}_\eta \right. \\ \left. + \left( \frac{\sigma \mathcal{P}\alpha \bar{T}\gamma}{\bar{\rho} F_\gamma} \right) k^4 \mathcal{U}_\eta \mathcal{U}_\kappa \right] w^{\text{BL}}(\xi) = 0. \quad (80)$$

Although the full equation for  $w^{\text{BL}}(\xi)$  is, of course, of the sixth order, inclusion of higher derivatives in (80) does not lead to any asymptotically distinguished balance. The corresponding MF equation at the leading order, i.e., outside the BL, is simply constructed of the last term in (80) without the derivative of the vertical velocity equated to zero,  $[\dots]w^{\text{MF}}(z) = 0$ , where the growth rate  $\sigma$  is a number and the rest of the terms in the square brackets are height-dependent functions. In this sense, the problem corresponds directly to that previously analyzed, so the only way to satisfy the MF equation for the most unstable mode is that  $w^{\text{MF}}(z)$  vanishes everywhere in the MF and it is allowed to be non-zero only in the vicinity of point  $z_{\text{max}}$ , where the square bracket  $[\dots]$  vanishes, i.e., the leading-order term of the entire  $z$ -dependent function in the square bracket is equal to  $-\sigma^3$ . Again, here we will concentrate on the most unstable mode only, and therefore do not consider oscillatory modes because they never grow at the highest rate in the analyzed problem.

In the BL Equation (80), all basic-state functions are evaluated at  $z = z_{\text{max}}$ , e.g.,  $\bar{\rho} \equiv \bar{\rho}(z_{\text{max}})$ ,  $F \equiv F(z_{\text{max}})$ , etc. Thus, all the coefficients in both the square brackets are constant at the leading order. Equation (80) was obtained in the asymptotic limit defined by  $k \gg 1$ ,  $\mathcal{U}_\kappa \ll 1$ ,  $\mathcal{U}_\eta \sim \mathcal{U}_\kappa^{3/2} \ll 1$ , and  $\delta(\mathcal{U}_\kappa, \mathcal{U}_\eta) \ll 1$ . As previously, we expect the power-law relation between the wavenumber and the small diffusivity parameters of the system, which due to the simplifying

assumption  $\mathcal{U}_\eta \sim \mathcal{U}_\kappa^{3/2}$  can be expressed solely in terms of  $\mathcal{U}_\kappa$ ,

$$k \sim \mathcal{U}_\kappa^{-1/n}, \quad \delta \sim \mathcal{U}_\kappa^{m/n} \sim k^{-m}, \quad (81)$$

for some  $n > 0$  and  $m > 0$ . The relation  $k \sim \mathcal{U}_\kappa^{-1/n}$  expresses only the order of magnitude of the wavenumber, because the same order can be achieved through a product of different powers of both diffusivities by the use of  $\mathcal{U}_\eta \sim \mathcal{U}_\kappa^{3/2}$ . Under the stated assumptions, all the terms proportional to the first derivative of  $w^{\text{BL}}(\xi)$  and derivatives higher than second are always negligible at the leading order. Equation (80) constitutes an eigenvalue problem for  $w(z)$  with an eigenvalue  $\sigma$ , similarly as in Section 3.

The main aim is to find the relation between large wavenumber  $k$  and the diffusivities  $\mathcal{U}_\kappa$  and  $\mathcal{U}_\eta$  for the most unstable mode, as well as its growth rate  $\sigma$  and the structure at the leading order. To this end, we need to consider the BL Equation (80) in all ranges of values of the exponents  $n$  and  $m$  for which the approximate form of the equation is different. In the same way as in Appendix A, it can be shown that for  $m \geq 1$  and any  $n > 0$ , we can only obtain solutions that do not satisfy the imposed boundary conditions and the requirement of smoothness, nor do they lead to specification of  $\sigma_0$ . Hence, here we only study cases with  $m < 1$  i.e.,  $\mathcal{U}_\kappa^{1/n} \ll \delta \ll 1$ .

To derive the expression for the leading-order term of the growth rate  $\sigma_0$ , we need to expand  $\sigma$  in powers of  $\delta$ , i.e.,  $\sigma = \sigma_0 + \delta\sigma_1 + \delta^2\sigma_2 + \dots$ , and then consider all possible different cases for any  $n > 0$ . Eventually, the mixture of numerical and theoretical analysis allows us to conclude that there are only two subintervals of  $n \in (0, +\infty)$  that lead to interesting distinct regimes with different growth rates of the most unstable modes:

1. For  $4/3 \leq n < 2$ , Equation (80) at the leading order takes the following form for the most unstable mode:  $[\sigma_0^2 - \sigma^2(z_{0,\text{max}})]w^{\text{BL}}(\xi) = 0$ , which leads to  $\sigma_0 = \sigma(z_{0,\text{max}})$  if we require non-trivial solutions;  $z_{0,\text{max}}$  is the point where the function  $\sigma(z)$  has its maximum. We have the same criterion for instability as in the isothermal case with or without magnetic diffusion, namely Equation (21). However, now the function  $F(z)$  depends on the basic-state temperature as was mentioned above. This regime is observed in numerical solutions at the values of  $k$  reaching  $k \sim 5 \times 10^4$  (which would correspond to waves as short as 1 km in the tachocline context). However, as demonstrated below, this is not a truly asymptotic regime. Rather, it results from a balance between terms in Equation (80) that are asymptotically small with terms that are asymptotically of order unity, but for the chosen basic state turn out to be significantly smaller than unity. Nevertheless, this limit is clearly shown to exist, and in fact is physically interesting, because it already corresponds to very large wavenumbers. A truly asymptotic regime is obtained either for  $n = 4/3$  or  $n > 2$ , but the former case may require physically unachievable large values of  $k$ .
2. For  $n > 2$ , Equation (80) at the leading order for the most unstable mode takes a different form:  $[\sigma_0^2 - \sigma_T^2(z_{T,\text{max}})]w^{\text{BL}}(\xi) = 0$ , which leads to  $\sigma_0 = \sigma_T(z_{T,\text{max}})$ , but now  $z_{T,\text{max}}$  is the point where the function  $\sigma_T(z)$  has its maximum. Thus, by (33) and (40), we have a new criterion for instability, namely Equation (43).

Other possible regimes corresponding to different ranges of the exponent  $n$ , which do not lead to the most unstable modes, are:

1. For  $n < 4/3$ , Equation (80) at the leading order takes the following form:  $\sigma_0 w^{\text{BL}}(\xi) = 0$ , which does not lead to unstable modes.
2. For  $n = 2$ , Equation (80) at the leading order yields:

$$\left[ \sigma_0(\sigma_0^2 - \sigma_T^2(z_0)) + \frac{\gamma F}{\rho F_\gamma} \mathcal{U}_\kappa k^2 (\sigma_0^2 - \sigma^2(z_0)) \right] w^{\text{BL}}(\xi) = 0, \quad (82)$$

which allows to determine  $\sigma_0$ . However, in this case it can be shown that, for any positive  $\Re e(\sigma_0)$  and any  $0 \leq z_0 \leq 1$ , the following inequalities are satisfied:  $0 < \Re e(\sigma_0) \leq \sigma(z_0)$  and  $0 < \Re e(\sigma_0) \leq \sigma_T(z_0)$ , where equality is possible if and only if  $\Re e(\sigma_0) = \sigma_T(z_0) = \sigma(z_0)$ . Thus, for  $n = 2$ , the growth rate can not correspond to the most unstable mode, except for the case when the maximal values of both the growth-rate functions  $\sigma_T(z_{\text{max}})$  and  $\sigma(z_{\text{max}})$  are equal, which can only be realized for a unique set of values of the physical parameters of the system (or in other words a very specific basic state), if it is possible at all, because  $\sigma_T(z) \neq \sigma(z)$  in general. This situation is, therefore, not considered physically realizable.

By the use of (39) and (40), one can derive a condition that must be satisfied in order for one of the two possible highest growth rates to dominate, namely

$$\begin{aligned} -H_T^{-1} > \frac{(\gamma - 1)}{F_\gamma} &\Leftrightarrow \sigma_T(z) > \sigma(z) \\ &\Rightarrow \sigma_T(z_{T,\text{max}}) > \sigma(z_{0,\text{max}}), \end{aligned} \quad (83)$$

where  $z_{T,\text{max}}$  and  $z_{0,\text{max}}$  are the points at which the growth-rate functions  $\sigma_T(z)$  and  $\sigma(z)$  take their respective maximum values. We use  $z_{\text{max}}$  to denote the point where the most unstable mode is localized; therefore,  $0 \leq z_{\text{max}} \leq 1$  can be equal to either  $z_{T,\text{max}}$ ,  $z_{0,\text{max}}$ , or neither of those, if the growth rate of the most unstable mode at the leading order happens to be different than  $\sigma_T(z_{T,\text{max}})$  and  $\sigma(z_{0,\text{max}})$ . It is clear, therefore, that if the temperature gradient is strong enough, the most unstable mode will be the one associated with the growth-rate function  $\sigma_T(z)$ . However, we emphasize that there exist situations in which, e.g.,  $\sigma_T(z_{T,\text{max}}) > \sigma(z_{0,\text{max}})$  even if the left inequality in (83) is not satisfied at every  $z$ , because  $z_{0,\text{max}} \neq z_{T,\text{max}}$  in general. Nevertheless, if  $\sigma_T(z_{T,\text{max}})$  is greater than  $\sigma(z_{0,\text{max}})$ , the most unstable mode is always associated with the growth rate  $\sigma_T(z_{T,\text{max}})$  at the leading order and  $n > 2$ . If, however,  $\sigma_T(z_{T,\text{max}}) < \sigma(z_{0,\text{max}})$ , the truly asymptotic regime is achieved either for  $n = 4/3$  with a growth rate of  $\sigma_{4/3}(z_{\text{max}}) = \sqrt{\sigma^2(z_{\text{max}}) + (k^2 \mathcal{U}_\eta \alpha \mathcal{P} \bar{T} / 2F)^2} - k^2 \mathcal{U}_\eta \alpha \mathcal{P} \bar{T} / 2F$  or for  $n > 2$  when, despite the relation between the maxima of the two growth-rate functions,  $\sigma_T(z_{T,\text{max}}) < \sigma(z_{0,\text{max}})$ , the most unstable mode still has a growth rate of  $\sigma_T(z_{T,\text{max}})$ . However, in the latter case, i.e.,  $\sigma_T(z_{T,\text{max}}) < \sigma(z_{0,\text{max}})$ , there exists a distinguished limit, albeit not fully asymptotic, still achieved at very short wavelengths, which corresponds to  $4/3 < n < 2$  and the growth rate  $\sigma(z_{0,\text{max}})$  of the most unstable mode.

We now turn to the subcases  $4/3 < n < 2$ ,  $n = 4/3$ , and  $n > 2$  and study them separately with an approach analogous to the one presented in Appendix A. We assume, that the growth rate function, which corresponds to the most unstable mode (either (39), (40) or  $\sigma_{4/3}$  has a quadratic maximum at  $z_{\max}$  and  $0 < z_{\max} < 1$ . Hence, at  $z_{\max}$ , the first derivative of one of the three growth rate functions is equal to zero and the second derivative is negative by assumption. The aim of the further analysis is to obtain the expression for the leading-order correction to the growth rate, the form of the most unstable mode, and the magnitude of its horizontal wavelength.

### B.1. Case $4/3 < n < 2$

The most unstable mode can be obtained for  $n < 2$  only when  $\sigma(z_{0,\max}) > \sigma_T(z_{T,\max})$ , which is a requirement for the basic state. Under such conditions, there are in fact two asymptotic regimes leading to distinguished limits, one for  $n = 4/3$  and a second one, out of the bounds  $4/3 < n < 2$ , for  $n = 3$ . However, we postpone the presentation of fully asymptotic solutions for later and start by considering a limit, which although it does not correspond to a fully asymptotic solution, nevertheless is the only one that could be observed in numerical simulations of the considered regime  $\sigma(z_{0,\max}) > \sigma_T(z_{T,\max})$  (see the next section), for  $\mathcal{U}_\kappa$  and  $\mathcal{U}_\eta$  as low as  $10^{-8}$  and  $10^{-12}$ , respectively, and  $k_{\max}$  as large as  $5.5 \times 10^4$ . This limit is determined by  $n = 5/3$  and  $m = 1/2$ , i.e.,  $k \sim \mathcal{U}_\kappa^{-3/5}$  and  $\delta \sim k^{-1/2} \sim \mathcal{U}_\kappa^{3/10}$ , and  $\sigma = \sigma_0 + k^{-1/2}\sigma_1 + k^{-1}\sigma_2 + \dots$ . In such a regime, from (80) at leading order, one obtains

$$\sigma_0^2 \frac{d^2}{d\xi^2} w^{\text{BL}}(\xi) + (\sigma_0^2 - \sigma^2(z_{0,\max})) w^{\text{BL}}(\xi) = 0, \quad (84)$$

and as in the case of (69), this leads to  $\sigma_0 = \sigma(z_{0,\max})$ , such that at the leading order, the growth rate of the most unstable mode is determined by the maximal value of the function  $\sigma(z)$ . Next, as before, we expand all the  $z$ -dependent functions in (80) about  $z_{0,\max}$ . Because the numerical solutions suggest  $\sigma(\sigma^2 - \sigma_T^2(z_{0,\max})) \ll 1$  and  $(\sigma_0^2 - ((\gamma - 1)H_\rho^{-1} - H_T^{-1})/\gamma)/(1 + \chi_\gamma) \ll 1$ , the BL equation at the next orders takes the form

$$\begin{aligned} 0 = & \frac{\sigma_0^2 \gamma F}{\bar{\rho} F_\gamma} k \mathcal{U}_\kappa \frac{d^2}{d\xi^2} w^{\text{BL}}(\xi) \\ & + \frac{\gamma F}{\bar{\rho} F_\gamma} \left( \sigma_1^2 + 2\sigma_0\sigma_2 - \frac{1}{2} \xi^2 \frac{d^2}{dz^2} \sigma^2(z) \Big|_{z=z_{0,\max}} + \mathcal{G}(z_{0,\max}) \right) k \mathcal{U}_\kappa w^{\text{BL}}(\xi) \\ & + \left[ \sigma_0(\sigma_0^2 - \sigma_T^2(z_{0,\max})) + \frac{2\gamma F}{\bar{\rho} F_\gamma} \sigma_0 \sigma_1 k^{3/2} \mathcal{U}_\kappa \right. \\ & \left. + \frac{\sigma_0 \mathcal{P} \alpha \bar{T} \gamma}{\bar{\rho} F_\gamma} k^4 \mathcal{U}_\eta \mathcal{U}_\kappa \right] w^{\text{BL}}(\xi), \end{aligned} \quad (85)$$

where all the  $z$ -dependent functions are evaluated at  $z = z_{0,\max}$ . The distinguished balance occurs at the order  $k^{-2/3}$  between the first two terms in (85), i.e., the second derivative term and the one proportional to  $k \mathcal{U}_\kappa w^{\text{BL}}(\xi)$ . The function  $\mathcal{G}(z_{0,\max})$  gathers all the contributions from terms at the order  $k^{-1/6}$  resulting

from Taylor expansions of all the terms in (80). On the other hand, the entire expression in the braces in (85) corresponds to the dominant order  $k^{-1/6}$ , and therefore has to be balanced separately, thus establishing the value of the correction  $\sigma_1$ . In writing the above, guided by our numerical simulations (cf. the next section), we have assumed that the properties of the basic state are such that  $\sigma(z_{0,\max})(\sigma^2(z_{0,\max}) - \sigma_T^2(z_{0,\max}))$  and  $(\sigma^2(z_{0,\max}) - ((\gamma - 1)H_\rho^{-1} - H_T^{-1})/\gamma)/(1 + \chi_\gamma)$  both happen to be as small as  $k^{-1/6} \sim \mathcal{U}_\kappa^{1/10}$ .<sup>2</sup> Therefore, as in all the previous cases of ‘‘body modes,’’ the structure of the most unstable mode is Gaussian-like, i.e., determined by the parabolic cylinder function.

As explained, the above solution requires basic-state functions, which are asymptotically of order unity, to enter a balance at an asymptotically small order. This can happen only in a limit where the final asymptotics has not set in yet. Despite the fact that the true asymptotic solutions may require wavelengths that are unphysically short, it is of interest to demonstrate the fully asymptotic solutions.

### B.2. Case $n = 4/3$

The analysis shows that, in the non-isothermal limit with  $\mathcal{U}_\kappa \neq 0$ ,  $\mathcal{U}_\eta \neq 0$ , and  $\mathcal{U}_\eta \sim \mathcal{U}_\kappa^{3/2} \ll 1$ , there are no asymptotic solutions for the most unstable mode with the growth rate determined solely by the function  $\sigma(z)$ . However, if the following conditions are satisfied, i.e.,  $\sigma(z_{0,\max}) > \sigma_T(z_{T,\max})$  as well as  $\sigma_{4/3}(z_{\max}) > \sigma_T(z_{T,\max})$ , the only distinguished limit at  $k \rightarrow \infty$  is the one leading to  $k^2 \mathcal{U}_\eta \sim 1$  and a leading-order balance between the terms  $\sim k^2 \mathcal{U}_\kappa$  and  $\sim k^4 \mathcal{U}_\eta \mathcal{U}_\kappa$  in (80) that corresponds to  $n = 4/3$ , i.e.,  $k \sim \mathcal{U}_\kappa^{-3/4}$ ,  $\delta \sim k^{-1/2} \sim \mathcal{U}_\kappa^{3/8}$ ,  $\sigma = \sigma_0 + k^{-2/3} \sigma_1 + k^{-1} \sigma_2 + \dots$ , and  $\sigma_0 = \sigma_{4/3}(z_{\max})$ , where  $z_{\max}$  is the point where the function  $\sigma_{4/3}(z_{\max})$  has its maximum value. The structure of the most unstable mode is, again, similar to all the previous cases described by the parabolic cylinder function. However, now the growth rate at the leading order is decreased with respect to  $\sigma(z_{0,\max})$ . Note that, for all  $z$  in the domain,  $\sigma_{4/3}(z) < \sigma(z)$ .

It is also interesting to note that, in the specific case of vanishing magnetic diffusivity (namely with  $\mathcal{U}_\eta = 0$  but  $\mathcal{U}_\kappa \neq 0$ ) described in Appendix C, no influence of thermal diffusivity on the most unstable modes is reported for  $\sigma(z_{0,\max}) > \sigma_T(z_{T,\max})$ , hence the thermal diffusion does not establish a finite wavenumber and the modes become more unstable with increasing wavenumber, i.e.,  $\sigma(k) \xrightarrow{k \rightarrow \infty} \sigma_0 = \sigma(z_0)$ . Therefore, when  $\sigma(z_{0,\max}) > \sigma_T(z_{T,\max})$  is satisfied, it is the presence of magnetic diffusion that allows to establish the wavelength of the most unstable mode in the range  $4/3 < n < 2$ , and thus for modes with a growth rate other than  $\sigma_T(z_{T,\max})$  occurring for  $n = 3$ , as demonstrated in Appendix B.3. However, when  $\sigma(z_{0,\max}) > \sigma_T(z_{T,\max})$ , but at the same time  $\sigma_{4/3}(z_{\max}) < \sigma_T(z_{T,\max})$ , the dominant fully

<sup>2</sup> Note that another distinguished balance is, in fact, possible for  $n = 5/3$ , with  $\sigma = \sigma_0 + k^{-2/3} \sigma_1 + k^{-1} \sigma_2 + \dots$  which requires  $\sigma(z_{0,\max})(\sigma^2(z_{0,\max}) - \sigma_T^2(z_{0,\max})) \sim k^{-1/3} \sim \mathcal{U}_\kappa^{1/5}$ . Although the above solution with  $\sigma = \sigma_0 + k^{-1/2} \sigma_1 + k^{-1} \sigma_2 + \dots$  is less restrictive for the basic state, as it requires the basic-state functions to be only of the order  $k^{-1/6}$ , it is not entirely clear which of these two limits sets in as a numerical solution; it is mainly determined by the order of magnitude of the expression  $\sigma(z_{0,\max})(\sigma^2(z_{0,\max}) - \sigma_T^2(z_{0,\max}))$ , either  $k^{-1/6}$  or  $k^{-1/3}$ . However, in both of the limits, we get  $k \sim \mathcal{U}_\kappa^{-3/5}$ ,  $\sigma_0 = \sigma(z_{0,\max})$  and the structure of the most unstable mode is very similar, with a slightly different function  $\mathcal{G}(z_{0,\max})$ .

asymptotic mode corresponds to the growth rate  $\sigma_T(z_{T,\max})$  and  $n = 3$ , just like when  $\sigma(z_{0,\max}) < \sigma_T(z_{T,\max})$ , which are the cases we turn to now.

### B.3. Case $n > 2$

The most unstable mode corresponds to  $n > 2$  when  $\sigma_T(z_{T,\max}) > \sigma_{4/3}(z_{\max})$  is satisfied, a condition resulting from the form of the basic-state solution. In such a case, the growth rate at the leading order,  $\sigma_0$ , is equal to  $\sigma_T(z_{T,\max})$  and the wavenumber is bounded from above by  $k \ll \mathcal{U}_\kappa^{-1/2}$ . Moreover, it can be shown that, for the most unstable mode,  $\sigma_1 = 0$ , and thus  $\sigma = \sigma_0 + \delta^2 \sigma_2 + o(\delta^2)$ . Hence, Equation (80) takes the following form

$$\begin{aligned} & \left[ \sigma_0 \left( 2\sigma_0 \sigma_2 \delta^2 - \frac{1}{2} \xi^2 \delta^2 \frac{d^2}{dz^2} \sigma_T^2(z) \right) \Big|_{z=z_{T,\max}} \right. \\ & \left. + \left( \frac{\gamma F}{\bar{\rho} F_\gamma} \right) \mathcal{U}_\kappa k^2 (\sigma_0^2 - \sigma^2(z_{T,\max})) \right] w^{\text{BL}}(\xi) \\ & - [\sigma_0^3 k^{-2} \delta^{-2}] \frac{d^2}{d\xi^2} w^{\text{BL}}(\xi) = 0. \end{aligned} \quad (86)$$

The structure of the equation is very similar to (70), but here we do not have the fourth-order derivative. Regardless of that, the analysis is exactly the same and it can be easily shown that, for any  $0 < m < 1$ , the most unstable mode will occur for  $n = 3$  and  $m = 1/2$ . Hence, we have  $k \sim \mathcal{U}_\kappa^{-1/3}$  and  $\delta \sim \mathcal{U}_\kappa^{1/6}$ . The correction  $\sigma_2$  to the growth rate has following form

$$\begin{aligned} \sigma_2 = & -\frac{1}{2\sqrt{2}} k^{-1} \delta^{-2} \sqrt{-\frac{d^2}{dz^2} \sigma_T^2(z) \Big|_{z=z_{T,\max}}} \\ & - \left( \frac{\gamma F}{2\bar{\rho} F_\gamma} \right) \mathcal{U}_\kappa k^2 \delta^{-2} \sigma_0^{-2} (\sigma_0^2 - \sigma^2(z_{T,\max})). \end{aligned} \quad (87)$$

This leads to the following expression for the growth rate of the most unstable mode

$$\begin{aligned} \sigma = & \sigma_0 - \frac{1}{2\sqrt{2}} k^{-1} \sqrt{-\frac{d^2}{dz^2} \sigma_T^2(z) \Big|_{z=z_{T,\max}}} \\ & - \left( \frac{\gamma F}{2\bar{\rho} F_\gamma} \right) \mathcal{U}_\kappa k^2 \sigma_0^{-2} (\sigma_0^2 - \sigma^2(z_{T,\max})) + o(\mathcal{U}_\kappa^{1/3}), \end{aligned} \quad (88)$$

where  $\sigma_0 = \sigma_T(z_{T,\max})$ . When compared to the expression (23), the growth rate (88) contains a derivative of a different growth-rate function, the one specific for the non-isothermal case, the most unstable mode is localized around different point,  $z_{T,\max}$ , and the diffusive correction is also different. In this case, the magnitude of the wavenumber  $k$ , established by the thermal diffusivity, is of the order  $\mathcal{U}_\kappa^{-1/3}$ . This most unstable eigenmode at the leading order takes the following form:

$$\begin{aligned} w_0(z) = & w^{\text{MF}}(z) + w^{\text{BL}}(z = \xi\delta + z_0) - w^{\text{match}}(z) \\ = & C \exp \left( -\frac{1}{2\sqrt{2}} k \sigma_0^{-1/2} \left( -\frac{d^2}{dz^2} \sigma_T^2(z) \Big|_{z=z_0} \right)^{1/4} (z - z_0)^2 \right), \end{aligned} \quad (89)$$

where  $C$  is an undetermined constant. The structure of this function is similar to the most unstable modes from previous cases, but the eigenmode (89) is localized in the vicinity of  $z_0 = z_{T,\max}$  and, as previously stated, the order of magnitude of the wavenumber is now  $k \sim \mathcal{U}_\kappa^{-1/3}$ .

## Appendix C

### Analysis of Equation (B29) for $\mathcal{U}_\eta = 0$ , $\mathcal{U}_\kappa \ll 1$ and $\sigma(z_{0,\max}) > \sigma_T(z_{T,\max})$

It is also of interest to consider the case with the extracted influence of sole thermal effects on the stability of the analyzed system (ergo in the absence of electrical resistivity).

For  $n < 2$  and  $\mathcal{U}_\eta = 0$ , Equation (80) at some  $z = z_0$  takes the following form

$$\begin{aligned} & \left[ \sigma_0 (\sigma_0^2 - \sigma_T^2(z_0)) + \left( \frac{\gamma F(z_0)}{\bar{\rho} F_\gamma(z_0)} \right) \mathcal{U}_\kappa k^2 \right. \\ & \left. \times \left( 2\sigma_0 \sigma_2 \delta^2 - \frac{1}{2} \xi^2 \delta^2 \frac{d^2}{dz^2} \sigma^2(z) \Big|_{z=z_0} \right) \right] w^{\text{BL}}(\xi) \\ & - \left[ \left( \frac{\gamma F(z_0)}{\bar{\rho} F_\gamma(z_0)} \right) \sigma_0^2 \mathcal{U}_\kappa \delta^{-2} \right] \frac{d^2}{d\xi^2} w^{\text{BL}}(\xi) = 0. \end{aligned} \quad (90)$$

It can be shown that, for any  $0 < m < 1$ , the only distinguished balances are

1.  $n < 1$  and  $m = 1/2$ . Hence, we have  $k \sim \mathcal{U}_\kappa^{-1/n} \gg \mathcal{U}_\kappa^{-1}$  and  $\delta \sim \mathcal{U}_\kappa^{1/2n} \ll \mathcal{U}_\kappa^{1/2}$ ; Equation (90) takes the form

$$\begin{aligned} & [k^{-2} \delta^{-4} \sigma_0^2] \frac{d^2}{d\xi^2} w^{\text{BL}}(\xi) \\ & - \left[ 2\sigma_0 \sigma_2 - \frac{1}{2} \xi^2 \frac{d^2}{dz^2} \sigma^2(z) \Big|_{z=z_0} \right] w^{\text{BL}}(\xi) = 0, \end{aligned} \quad (91)$$

which has the same structure as Equation (71), and thus leads to a similar result:

$$\sigma_2 = -\frac{1}{2\sqrt{2}} k^{-1} \delta^{-2} \sqrt{-\frac{d^2}{dz^2} \sigma^2(z) \Big|_{z=z_0}}. \quad (92)$$

2.  $n = 1$  and  $m = 1/2$ . Here, we have  $k \sim \mathcal{U}_\kappa^{-1}$  and  $\delta \sim \mathcal{U}_\kappa^{1/2}$ ; Equation (90) takes the form

$$\begin{aligned} & \left[ \left( \frac{\bar{\rho} F_\gamma(z_0)}{\gamma F(z_0)} \right) \mathcal{U}_\kappa^{-1} k^{-2} \delta^{-2} \sigma_0 (\sigma_0^2 - \sigma_T^2(z_0)) \right. \\ & \left. + 2\sigma_0 \sigma_2 - \frac{1}{2} \xi^2 \frac{d^2}{dz^2} \sigma^2(z) \Big|_{z=z_0} \right] w^{\text{BL}}(\xi) \\ & - [k^{-2} \delta^{-4} \sigma_0^2] \frac{d^2}{d\xi^2} w^{\text{BL}}(\xi) = 0, \end{aligned} \quad (93)$$

which has the same structure as Equation (73), hence

$$\begin{aligned} \sigma_2 = & -\frac{1}{2\sqrt{2}} k^{-1} \delta^{-2} \sqrt{-\frac{d^2}{dz^2} \sigma^2(z) \Big|_{z=z_0}} \\ & - \left( \frac{\bar{\rho} F_\gamma(z_0)}{2\gamma F(z_0)} \right) \mathcal{U}_\kappa^{-1} k^{-2} \delta^{-2} (\sigma_0^2 - \sigma_T^2(z_0)). \end{aligned} \quad (94)$$

In both cases,  $\sigma_2 < 0$  and  $|\sigma_2| \sim 1$ . However, the thickness of the BL  $\delta$  is asymptotically smaller for the first case:  $\delta_{n < 1} \ll \delta_{n=1}$ . Therefore, if  $\sigma = \sigma_0 - \delta^2|\sigma_2| + o(\delta^2)$ , it can be seen that, for  $n < 1$ , the growth rate  $\sigma_{n < 1}$  is asymptotically greater than  $\sigma_{n=1}$  obtained for  $n = 1$ . This leads to a conclusion that the former case gives the most unstable mode with the growth rate

$$\sigma = \sigma_0 - \frac{1}{2\sqrt{2}}k^{-1}\sqrt{-\frac{d^2}{dz^2}\sigma^2(z)}\Big|_{z=z_0} + o(\mathcal{U}_\kappa^{1/n}), \quad (95)$$

where  $z_0 = z_{0,\max}$ . This result is similar to the one obtained in Mizerski et al. (2013) for an isothermal case without dissipation. The only difference is the inclusion of the  $\bar{T}(z)$  function in the latter formula. This means that, for  $\sigma(z_{0,\max}) > \sigma_T(z_{T,\max})$ , the finite magnitude of the wavenumber  $k$  is not established by the thermal diffusivity  $\mathcal{U}_\kappa$ . Moreover, there is no explicit dependence of  $\sigma$  on  $\mathcal{U}_\kappa$ , at least within the accuracy of terms of the order  $\mathcal{U}_\kappa^{1/n}$ . Thus, the most unstable modes are those with  $k \rightarrow \infty$  (which means  $n \rightarrow 0$ ), and obviously  $\sigma \rightarrow \sigma(z_{0,\max})$ . The leading-order approximation for the most unstable mode takes following form

$$w_x(z) = C \exp\left(-\frac{(z-z_0)^2}{2\sqrt{2}}k\sigma_0^{-1/2}\left(-\frac{d^2}{dz^2}\sigma^2(z)\Big|_{z=z_0}\right)^{1/4}\right), \quad (96)$$

where  $C$  is an undetermined constant. The structure of this function is similar to the most unstable mode in the case with only magnetic diffusion, but no thermal diffusion.

Finally, just like in Appendix B.3, when  $\sigma(z_{0,\max}) < \sigma_T(z_{T,\max})$ , the most unstable mode corresponds to  $n = 3$  and is described by  $\sigma_0 \approx \sigma_T(z_{T,\max})$  and  $k \sim \mathcal{U}_\kappa^{-1/3}$ .

## Appendix D

### Details of the 3D Asymptotic Analysis for $\mathcal{U}_\eta \sim \mathcal{U}_\kappa^{3/2} \ll 1$

To derive expressions for the leading-order term of the growth rate in the 3D case, Equations 45(a)–(j) are analyzed locally in the limit  $k_y \gg 1$  via the use of the boundary/internal layer approach—namely in terms of the local variable  $\xi$  (expanding the growth rate and all depth-dependent functions in powers of  $\delta$ ). All possible different cases for any  $n > 0$  with  $k_y \sim \mathcal{U}_\kappa^{-1/n}$  can be considered similarly as in Section 4, but let us concentrate only on the case where the partly asymptotic solution with  $k_y \sim \mathcal{U}_\kappa^{3/5}$  is allowed (which seems natural, as confirmed by all our 2D numerical simulations). This allows for uniqueness because the partly asymptotic solution, when allowed, dominates in the range  $4/3 < n < 2$ , and the range  $n > 2$  is characterized by a different growth rate ( $\sigma_T$  in the 2D case). Therefore, under such circumstances, we obtain two distinct regimes with two different growth rates of the most unstable modes, denoted as  $\sigma_{3D}$  and  $\sigma_{T3D}$ .

#### D.1. The Most Unstable 3D Mode for $\sigma_{3D} > \sigma_{T3D}$

When the inequality  $\sigma_{3D} > \sigma_{T3D}$  is satisfied, the exponent  $n$  (where  $k_y \sim \mathcal{U}_\kappa^{-1/n}$ ) for the most unstable mode can be shown to fall into the range  $4/3 < n < 2$ . Thus, in the limit  $k_y \gg 1$ ,  $\mathcal{U}_\eta \ll 1$  and  $\mathcal{U}_\kappa \ll 1$ , the system of Equations 45(a)–(j) can be

transformed at the leading order into a second-order ODE for the vertical velocity perturbation in the local variable,  $w^{\text{BL}}(\xi)$ ,

$$\frac{d^2}{d\xi^2}w^{\text{BL}}(\xi) = \delta^2k_y^2(A_1A_2)^{-1}(\sigma^4 + A_1A_3\sigma^2 + A_1A_4)w^{\text{BL}}(\xi), \quad (97)$$

where the coefficients  $A_1$ ,  $A_2$ ,  $A_3$ , and  $A_4$  are constants dependent on the horizontal wavenumber  $k_x$  and contain the values of basic-state functions taken at a point  $z = z_0$ , which corresponds the region of localization of the most unstable mode, e.g.,  $\bar{\rho} \equiv \bar{\rho}(z_0)$ ,  $F \equiv F(z_0)$ , etc. They take the following form

$$A_1 = \left(\frac{\Lambda\bar{B}^2}{\bar{\rho}}\right)F^{-1} \equiv (\chi^{-1} + 1)^{-1}, \quad (98a)$$

$$A_2 = \left[\sigma^2\left(\frac{\Lambda\bar{B}^2}{\bar{\rho}}\right)^{-1} + k_x^2\right]\left[\sigma^2F + k_x^2\left(\frac{\Lambda\bar{B}^2}{\bar{\rho}}\right)^2\chi^{-1}\right], \quad (98b)$$

$$A_3 = k_x^2\left(\frac{\Lambda\bar{B}^2}{\bar{\rho}}\right)(2\chi^{-1} + 1) - (H_\rho^{-1} - H_B^{-1}), \quad (98c)$$

$$A_4 = k_x^2\left(\frac{\Lambda\bar{B}^2}{\bar{\rho}}\right)\left[k_x^2\left(\frac{\Lambda\bar{B}^2}{\bar{\rho}}\right)\chi^{-1} + H_B^{-1}\right], \quad (98d)$$

where  $F$  and  $\chi$  were defined in (32). The coefficients  $A_1$ – $A_4$  are similar to those in the Equation (64) in Mizerski et al. (2013), although our case is non-isothermal—and thus the basic-state temperature of the fluid is non-uniform. Hence, the growth rate of the most unstable mode at the leading order,  $\sigma_{3D,0}$ , is determined by the solution of the algebraic equation (“dispersion relation”)  $\sigma^4 + A_1A_3\sigma^2 + A_1A_4 = 0$  with the greatest real part. It takes the following form

$$\sigma_{3D,0}^2 = -\frac{A_1A_3}{2} + \frac{1}{2}[A_1(A_1A_3^2 - 4A_4)]^{1/2}. \quad (99)$$

As stated, we study only the case of stably stratified fluid, i.e.,  $H_\rho < 0$ . Therefore, just as in the isothermal and non-diffusive case studied in Mizerski et al. (2013), it can be shown from the “dispersion relation”  $\sigma^4 + A_1A_3\sigma^2 + A_1A_4 = 0$  that the instability sets in only as a direct mode with  $\sigma$  passing through zero, which implies  $A_1A_4 < 0$ . Thus, we obtain the criterion (46) for instability with respect to the 3D modes.

#### D.2. The Most Unstable 3D Mode for $\sigma_{T3D} > \sigma_{3D}$

When  $\sigma_{T3D} > \sigma_{3D}$ , the exponent  $n$  for the most unstable mode is in the range  $n > 2$ . In this regime, both the thermal and the magnetic diffusion are negligible at the leading order. Thus, in the limit  $k_y \gg 1$ ,  $\mathcal{U}_\eta \ll 1$ ,  $\mathcal{U}_\kappa \ll 1$ , the system of Equations 45(a)–(j) can be transformed at the leading order into one second-order ODE for the vertical velocity perturbation in the local variable,  $w^{\text{BL}}(\xi)$

$$\frac{d^2}{d\xi^2}w^{\text{BL}}(\xi) = \delta^2k_y^2(A_{1\gamma}A_{2\gamma})^{-1}(\sigma^4 + A_{1\gamma}A_{3\gamma}\sigma^2 + A_{1\gamma}A_{4\gamma})w^{\text{BL}}(\xi), \quad (100)$$

where constant coefficients  $A_{1\gamma}$ ,  $A_{2\gamma}$ ,  $A_{3\gamma}$ , and  $A_{4\gamma}$  depend on the horizontal wavenumber  $k_x$ . Their explicit forms are:

$$A_{1\gamma} = \left( \frac{\Lambda \bar{B}^2}{\bar{\rho}} \right) F_\gamma^{-1} \equiv (\chi_\gamma^{-1} + 1)^{-1}, \quad (101a)$$

$$A_{2\gamma} = \left[ \sigma^2 \left( \frac{\Lambda \bar{B}^2}{\bar{\rho}} \right)^{-1} + k_x^2 \right] \left[ \sigma^2 F_\gamma + k_x^2 \left( \frac{\Lambda \bar{B}^2}{\bar{\rho}} \right)^2 \chi_\gamma^{-1} \right], \quad (101b)$$

$$A_{3\gamma} = k_x^2 \left( \frac{\Lambda \bar{B}^2}{\bar{\rho}} \right) (2\chi_\gamma^{-1} + 1) - (H_\rho^{-1} - H_B^{-1}) + \chi^{-1} (H_T^{-1} - (\gamma - 1)H_\rho^{-1}), \quad (101c)$$

$$A_{4\gamma} = k_x^2 \left( \frac{\Lambda \bar{B}^2}{\bar{\rho}} \right) \left[ k_x^2 \left( \frac{\Lambda \bar{B}^2}{\bar{\rho}} \right) \chi_\gamma^{-1} + H_B^{-1} + \chi^{-1} (H_T^{-1} - (\gamma - 1)H_\rho^{-1}) \right], \quad (101d)$$



where  $F_\gamma$  and  $\chi_\gamma$  were defined in (31). The latter set of coefficients differs from the former with the presence of the  $\gamma$  parameter in the  $\chi$  function. Moreover, the parameters  $A_{3\gamma}$  and  $A_{4\gamma}$  also have an additional term containing the inverse temperature scale height  $H_T^{-1}$ , denoted by  $\mathcal{H}^{-1}$  in Section 6. This is a similar situation as in 2D case, cf. Equations (39) and (40).

Hence, the growth rate of the most unstable mode at the leading order,  $\sigma_{T3D,0}$ , is determined by the greatest solution of the algebraic equation (“dispersion relation”)  $\sigma^4 + A_{1\gamma}A_{3\gamma}\sigma^2 + A_{1\gamma}A_{4\gamma} = 0$  (and, similarly as before, it can be shown that  $A_{1\gamma}A_{4\gamma} < 0$ , so the growth rate is real and positive at the leading order). It takes the following form

$$\sigma_{T3D,0}^2 = -\frac{A_{1\gamma}A_{3\gamma}}{2} + \frac{1}{2} [A_{1\gamma}(A_{1\gamma}A_{3\gamma}^2 - 4A_{4\gamma})]^{1/2}. \quad (102)$$

This results in (48), the criterion for instability with respect to 3D modes.

## ORCID iDs

Marek J. Gradzki  <https://orcid.org/0000-0002-5115-251X>  
 Krzysztof A. Mizerski  <https://orcid.org/0000-0003-0106-675X>

## References

- Abramowitz, M., & Stegun, I. A. 1972, *Handbook of Mathematical Functions with Formulas, Graphs, and Mathematical Tables* (New York: Dover)
- Acheson, D. J. 1979, *SoPh*, **62**, 23
- Acheson, D. J. 1980, *JFM*, **96**, 723
- Acheson, D. J. 1983, *GApFD*, **27**, 123
- Bender, C. M., & Orszag, S. A. 1978, *Advanced Mathematical Methods for Scientists and Engineers* (New York: McGraw-Hill)
- Berkoff, N. A., Kersal, E., & Tobias, S. M. 2010, *GApFD*, **104**, 545
- Bowker, J. A., Hughes, D. W., & Kersal, E. 2014, *GApFD*, **108**, 553
- Cattaneo, F., Chiueh, T., & Hughes, D. W. 1990, *JFM*, **219**, 1
- Cattaneo, F., & Hughes, D. W. 1988, *JFM*, **196**, 323
- Choudhuri, A. R. 1998, *The Physics of Fluids and Plasmas* (Cambridge: Cambridge Univ. Press)
- Davies, C. R., & Hughes, D. W. 2011, *ApJ*, **727**, 112
- Friedlander, S. 1987, *GApFD*, **39**, 315
- Gilman, P. A. 1967a, *JAtS*, **24**, 101
- Gilman, P. A. 1967b, *JAtS*, **24**, 119
- Gilman, P. A. 1967c, *JAtS*, **24**, 130
- Gilman, P. A. 1967d, *JAtS*, **24**, 333
- Gilman, P. A. 1970, *ApJ*, **162**, 1019
- Gilman, P. A. 2014, *ApJ*, **787**, 60
- Gilman, P. A. 2015, *ApJ*, **801**, 22
- Gilman, P. A. 2017, *ApJ*, **842**, 2
- Gough, D. O. 2007, in *The solar Tachocline*, ed. D. W. Hughes, R. Rosner, & N. O. Weiss (Cambridge: Cambridge Univ. Press), 3
- Hughes, D. W. 1985, *GApFD*, **34**, 99
- Hughes, D. W. 1992, in *Sunspots: Theory and Observations*, ed. J. H. Thomas & N. O. Weiss (Dordrecht: Kluwer), 371
- Hughes, D. W. 2007, in *The solar Tachocline*, ed. D. W. Hughes, R. Rosner, & N. O. Weiss (Cambridge: Cambridge Univ. Press), 275
- Hughes, D. W., & Proctor, M. R. E. 1988, *AnRFM*, **20**, 187
- Kersal, E., Hughes, D. W., & Tobias, S. M. 2007, *ApJL*, **663**, L113
- Mizerski, K. A., Davies, C. R., & Hughes, D. W., 2013, *ApJS*, **205**, 16
- Newcomb, W. A. 1961, *PhFI*, **4**, 391
- Parker, E. N. 1955, *ApJ*, **121**, 491
- Parker, E. N. 1979, *Cosmical Magnetic Fields: Their Origin and Their Activity* (Oxford: Clarendon)
- Tobias, S. M., & Hughes, D. W. 2004, *ApJ*, **603**, 785